NASA/TM-20220008026

An Interim Assessment of High-Power-Density-Core Noise Levels

Lennart S. Hultgren
Glenn Research Center, Cleveland, Ohio

June 2022

NASA STI Program . . . in Profile

Since its founding, NASA has been dedicated to the advancement of aeronautics and space science. The NASA Scientific and Technical Information (STI) Program plays a key part in helping NASA maintain this important role.

The NASA STI Program operates under the auspices of the Agency Chief Information Officer. It collects, organizes, provides for archiving, and disseminates NASA's STI. The NASA STI Program provides access to the NASA Technical Report Server—Registered (NTRS Reg) and NASA Technical Report Server—Public (NTRS) thus providing one of the largest collections of aeronautical and space science STI in the world. Results are published in both non-NASA channels and by NASA in the NASA STI Report Series, which includes the following report types:

- TECHNICAL PUBLICATION. Reports of completed research or a major significant phase of research that present the results of NASA programs and include extensive data or theoretical analysis. Includes compilations of significant scientific and technical data and information deemed to be of continuing reference value. NASA counter-part of peer-reviewed formal professional papers, but has less stringent limitations on manuscript length and extent of graphic presentations.

- TECHNICAL MEMORANDUM. Scientific and technical findings that are preliminary or of specialized interest, e.g., "quick-release" reports, working papers, and bibliographies that contain minimal annotation. Does not contain extensive analysis.

- CONTRACTOR REPORT. Scientific and technical findings by NASA-sponsored contractors and grantees.

- CONFERENCE PUBLICATION. Collected papers from scientific and technical conferences, symposia, seminars, or other meetings sponsored or co-sponsored by NASA.

- SPECIAL PUBLICATION. Scientific, technical, or historical information from NASA programs, projects, and missions, often concerned with subjects having substantial public interest.

- TECHNICAL TRANSLATION. English-language translations of foreign scientific and technical material pertinent to NASA's mission.

For more information about the NASA STI program, see the following:

- Access the NASA STI program home page at http://www.sti.nasa.gov

- E-mail your question to help@sti.nasa.gov

- Fax your question to the NASA STI Information Desk at 757-864-6500

- Telephone the NASA STI Information Desk at 757-864-9658

- Write to:
  NASA STI Program
  Mail Stop 148
  NASA Langley Research Center
  Hampton, VA 23681-2199

NASA/TM-20220008026

An Interim Assessment of High-Power-Density-Core Noise Levels

Lennart S. Hultgren
Glenn Research Center, Cleveland, Ohio

National Aeronautics and
Space Administration

Glenn Research Center
Cleveland, Ohio 44135

June 2022

This work was sponsored by the Advanced Air Vehicle Program
at the NASA Glenn Research Center

Level of Review: This material has been technically reviewed by technical management.

This report is available in electronic form at http://www.sti.nasa.gov/ and http://ntrs.nasa.gov/

An Interim Assessment of High-Power-Density-Core Noise Levels

Lennart S. Hultgren
National Aeronautics and Space Administration
Glenn Research Center
Cleveland, Ohio 44135

Abstract

The aeroacoustic-noise implications associated with the small-core gas-turbine development effort underway in the NASA HyTEC Project are discussed. Due to the expected design choices, there are risks that the airport community noise, associated with landing and takeoff of civilian-transport aircraft, could be increased or, at minimum, that further overall propulsion-noise reduction could become limited. It is argued here that the main culprit in these scenarios is noise originating from sources in the combustor. The classical combustor-noise prediction model is summarized and its possible extension to the planned parameter space is discussed. An acoustic-power scaling law is derived and utilized to give initial estimates for what can be expected by core-design choices. An ideal-cycle parametric turbofan model provides input for these estimates.

1 Introduction

One of the strategic thrusts of the NASA Aeronautics Research Mission Directorate (ARMD) is to develop technologies and concepts to enable future environmentally sustainable ultra-efficient commercial air transport vehicles. This is critical in order to reduce the impact of aviation on the environment as this industry and the corresponding global transportation system continue to grow. Future propulsion systems are envisioned to have an increasingly higher bypass ratio from larger fans combined with much smaller cores, with high-efficiency, ultra-clean burning, fuel-flexible combustors [1]. This, in combination with expected aircraft configuration changes, and advances in fan-noise mitigation will change the propulsion-noise source balance, with core noise becoming an increasingly important, if not dominant, component. Furthermore, the noise impact of small, high-power-density cores is not only important to future gas-turbine propulsors, but also to envisioned hybrid-electric aircraft-propulsion systems.

Combustor noise is a low-frequency broadband component generated in the turbofan engine core and can make a significant contribution to the aft-quadrant overall noise signature at low-power conditions typical of approach for current-generation high-bypass-ratio turbofan engines. Of the core-noise sources (compressor, combustor, and turbine), combustor noise is potentially the one most negatively affected, i.e., increased in strength, by the expected turbofan-design changes. Consequently, if not further controlled, combustor noise may well set a noise floor limiting the impact of future noise-reduction achievements for other propulsion-noise sources.

Achieving both future emissions and community-noise goals will require improved combustor-noise source descriptions and prediction capability addressing mechanisms unique to future low-emissions combustor technology and high-power-density core designs. Such capability is essential for enabling accurate aircraft system-level community-noise projections and design trades at preliminary/conceptual design stages, for enabling detailed component-level technology development to address noise at the source through multi-disciplinary acoustics/emissions combustor design, as well as developing effective noise-mitigation techniques. These crucial issues are key elements in the strategy to develop novel propulsion systems for ultra-efficient transport aircraft.

The NASA Hybrid Thermally Efficient Core (HyTEC) Project currently is at the very beginning of its Phase-1 effort. The overall goal is to develop high-power-density-core engine technologies that achieve a 5- to 10-percent fuel burn benefit for early 2030s Entry-Into-Service (EIS) single-aisle aircraft versus corresponding 2020s-best-in-class transports. The required increase in thermal efficiency is expected to be accomplished through the integration of aerodynamic and material technologies. This challenge is relevant to two Key Subsonic-Transport Technologies (TRL 6[a] by 2025-28) identified by NASA, namely Small Core Gas Turbine (SCGT) and Electrified Aircraft Propulsion (EAP). Clearly core acoustics need to be an integral part of this effort.

[a] https://en.wikipedia.org/wiki/Technology_readiness_level – Retrieved March 1, 2022

2 Background

Since the introduction of turbofan aeroengines in the 1960s, their design has trended (and will so continue) towards an ever higher bypass ratio (BPR) as well as an increased overall-pressure-ratio (OPR), both for increased engine-performance reasons. The turbofan overall efficiency, in principle, increases with the BPR and a higher OPR leads to an increased core thermal efficiency, see Appendix A.[b] For a given core size, as measured by its mass flow rate, a higher BPR is accomplished by matching the core with a larger fan. However, for a given airframe design, there is a practical limit on how large a fan diameter can be used—the fan has to 'fit' on the airplane and nacelle drag increases with the fan diameter as well. This has resulted in technology development efforts, eg. HyTEC, to enable core-size reduction, while maintaining or increasing core 'power' output. Figure 1 illustrates these trends.

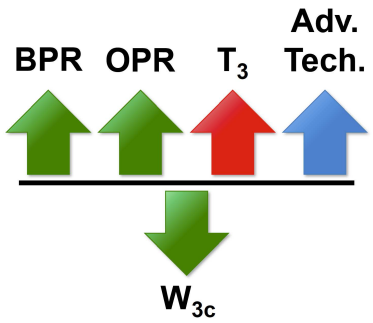

Figure 1. Turbofan Design Trends

The green arrow labeled W_{3c} indicates the reduced core mass flow rate for high-power-density-core designs. For this design choice, it is imperative that the core thermal efficiency is raised as the mass flow rate is decreased in order to achieve the required net increase in the kinetic energy flux in the core and fan streams, i.e., the OPR must be increased in this case. Because of the increased OPR, the compressor exit total temperature, T_3, will be higher. There are two major consequences: First, material challenges for the latter stages of the high-pressure compressor are likely; and, second, an increase in emissions from the combustion process is to be expected. To counteract these undesirable issues, as well as fluid mechanical challenges in narrow compressor passages, advanced aerodynamic, material, and combustor technologies need to be developed and applied. Combustor designs, in particular, are likely in the long run to move away from the current, well established, non-premixed rich-lean concepts toward premixed (or partially-premixed) lean-lean combustion. Lean-lean combustion, being inherently more unsteady than present common technology, presents greater challenges with respect to thermo-acoustic instabilities as well as the potential of a more significant contribution to airport community noise.

Some understanding of the effects of changes in turbofan design on airport-community-noise components can be obtained by comparing the results of two NASA system studies [2, 3], both from about a decade ago. The predicted effective perceived noise level (EPNL) at approach from the two studies are shown in Fig. 2.

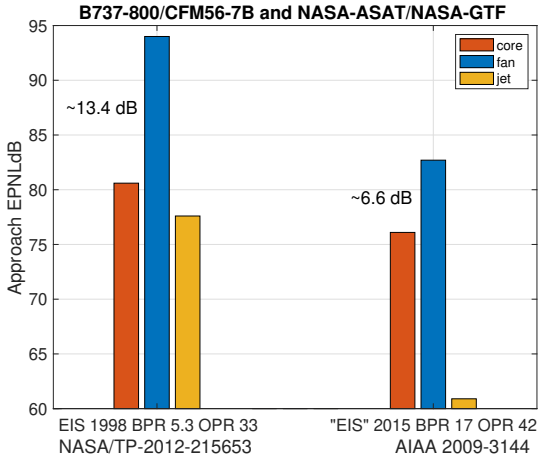

Figure 2. Predicted EPNL Contributions at Approach

The results [2] on the left in the figure are for a modern reference case consisting of a Boeing 737-800 airplane with CFM56-7B engines. The BPR is 5.3 and the OPR is 33 at the aerodynamical design point (ADP). This actual aircraft entered into service (EIS) in 1998. NASA [2] developed an engine representation in the Numerical Propulsion System Simulator (NPSS) [4] using certification data and other publicly available information. No proprietary data was used in the model. Acoustic predictions then could be obtained using the NASA Aircraft Noise Prediction Program (ANOPP) [5, 6]. For details see the NASA Technical Publication [2].

The results [3] on the right side are for a NASA advanced-concept aircraft: Advanced-Single-Aisle Transport (ASAT) with a Geared-Turbofan Engine (GTF). These are both NASA theoretical constructs and do not correspond to any existing airplane or engine. The technologies included in the models were

[b] Appendix A is included in the report as a courtesy to aeroacousticians that, even though having a general understanding of turbomachinery, might not have the covered details readily at hand.

determined by the envisioned 2015 EIS. The BPR is 17 and the OPR is 42 at the ADP. The noise predictions were obtained in an analogous manner to the B737/CFM56-7B scenario. For details see the AIAA paper [3].

Figure 2 shows that the BPR increase significantly reduces the jet noise-—as shown by the gold bars. The fan (blue bars) is the dominant noise source in both cases. However, its dominance is halved between the studies–from 13.4 dB to 6.6 dB above the core/combustor component (red bars). Both the fan and core components are reduced, but less so for the core noise. These trends are expected to continue, which means that, at some future point in time, core noise could become a limiting issue for further propulsion noise reduction.

3 HyTEC-Project High-Power-Density Small-Core Goals

As part of an overall NASA ARMD subsonic-transport strategic thrust to drastically reduce aircraft fuel burn and emissions, the HyTEC Project aims to develop and demonstrate, in partnership with industry, technologies for high-power-density, small-core gas turbines and electrified aircraft propulsion. The vision is to stimulate development, to accelerate industry adoption, and to expedite the fleet impact of new key propulsion technologies. A Request for Proposals (RFP) for a Phase-1 effort was released on May 29, 2021 as NASA Research Announcement (NRA) Solicitation 80GRC021N0001. The RFP listed two objectives: (i) demonstrate increased thermal efficiency with integrated high-power-density-core engine technologies achieving a 5- to 10-percent fuel-burn benefit, versus 2020 best in class, for early 2030s EIS single-aisle aircraft; and (ii) achieve up to 20-percent power-extraction at altitude from a modern commercial turbofan engine with the thrust, efficiency, operability, and durability to enable the benefits of electrified aircraft propulsion at the vehicle level. The potential acoustic implications of the first objective is the focus of the present report.

3.1 *HyTEC-Project Key Performance Parameters*

The RFP delineates several Measures of Effectiveness (MOE), Measures of Performance (MOP), and Key Performance Parameters (KPP) for the HyTEC Project. The first set, MOE, establishes expectations and goals against which the overall effectiveness of the effort is judged and the second group, MOP, outlines key steps and project objectives. Table 1, which is included here only for informational purposes, lists the MOEs and MOPs relevant to the present report.

Table 1. Select HyTEC-Project Measures of Effectiveness and Performance, NRA Solicitation 80GRC021N0001

MOE Number	Measure of Effectiveness
MOE-1	Define a viable path that identifies key high-power-density core technologies needed to accelerate U.S. Industry product that is enhanced by Government participation
MOE-2	Establish a turbofan engine with a high-power-density core that addresses the next generation single-aisle for EIS in the 2035 timeframe
MOP Number	**Measure of Performance**
MOP-2	Develop and demonstrate via ground test an advanced high-power-density core engine
MOP-3	Raise the TRL level of high-power-density-core technologies to TRL 4–5 through component testing by 2023
MOP-4	Raise the TRL level of high-power-density-core technologies to TRL 6 through ground testing by 2026

The third category, KPP, defines success criteria for the technology development. Of these, the KPP-1, KPP-2, KPP-3, and KPP-6 define the desired small-core turbofan parameter space, see Table 2.[c]

[c]The KPP wording has been slightly tweaked here for simplicity compared to the Solicitation 80GRC021N0001.

Table 2. Select HyTEC-Project Key Performance Parameters, NRA Solicitation 80GRC021N0001

KPP Number	Key Performance Parameter	Full Success	Minimum Success
KPP-1	Fuel burn reduction attributed to high-power-density core (of the original equipment manufacturer's vision turbofan engine)	10%	5%
KPP-2	Engine bypass ratio	> 15	> 12
KPP-3	Engine overall pressure ratio at top of climb	> 50	> 45
KPP-6	High-pressure-compressor exit corrected flow	< 3 lbm/s	< 3.5 lbm/s

3.2 *Ideal-Cycle Analysis and Comparison to a Reference Case*

In order to better understand the relationships between design parameters and performance requirements, it is useful to carry out an ideal-turbofan parametric cycle analysis. However, a reader well versed in cycle analysis may skip to the next section. For the convenience of other readers, the steps involved in an ideal-turbofan parametric cycle analysis are summarized in Appendix A. Combining the ideal parametric cycle analysis with performance requirements relative to a baseline engine then provides rough estimates for the needed (new) small-core design space. The CFM56-7B24 engine is chosen here[d] as baseline mainly because sufficient open information is available. Table 3 lists its specifications at the ADP, which is the top of climb (TOC) condition, i.e., the OPR, BPR, and fan pressure ratio (FPR) are given. The flight Mach number (M_0) at TOC is taken as the cruise Mach number of the Boeing 737-800 aircraft, i.e., 0.785.

Table 3. CFM56-7B24 at ADP

TOC	10.668 km (35-thousand feet)
OPR	32.7
BPR	5.3
FPR	1.55
M_0	0.785

While the HyTEC RFP does not specify a desired increase in the turbofan (or more precisely the core) thermal efficiency, it is assumed here that a 5-percent absolute increase in the thermal efficiency is needed to achieve the stated fuel-burn-reduction goal. For a turbofan (or turbojet) the ideal-cycle expression for the thermal efficiency (η_T) is given by Eq. (A 39), which shows that the ideal thermal efficiency increases with the overall compression ratio (OCR), The OCR is the product of the inlet ram compression and the total pressure ratio of the engine compression chain—that is from fan face to compressor exit—i.e., the OPR. The ram effect, see Eq. (A 20), basically is a function only of the flight Mach number. The blue curve in Fig. 3 shows the new- to baseline-OPR ratio as a function of the baseline OPR required to achieve a 5-percent increase in η_T with $M_0 = 0.785$ for both cases. Assuming the same cruise Mach number, the ideal parametric cycle analysis thus shows that the OPR must be raised to 58.3 to give a 5-percent absolute increase in the thermal efficiency relative to the baseline herein. This rough OPR estimate is in line with KPP-3.

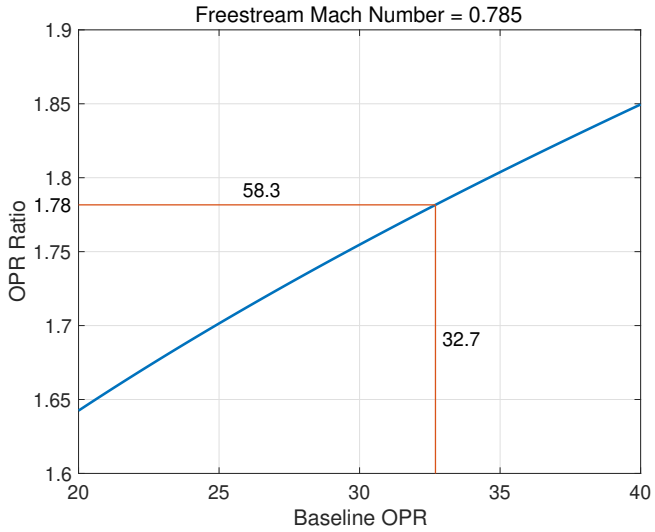

Figure 3. New- to Baseline-OPR Ratio Needed to Achieve a 5-percent Absolute Increase in η_T for a Fixed M_0 as a Function of Baseline OPR

The core size of turbofans traditionally is expressed in terms of corrected mass flow rate at the high-pressure-compressor (HPC) exit. The HyTEC-project goal in this respect is expressed by KPP-6. The corresponding corrected mass flow rate for the CFM56-7B baseline engine is not readily available in the literature and,

[d] It certainly can not be considered a 2020-best-in-class engine, but it is still an extensively used modern turbofan and was chosen as baseline for the given reason.

consequently, has to be estimated. However, a stated maximum flow of 752 lbm/s (341 kg/s) for the CFM56-7B24 (the engine developed for the Boeing 737-800) can be found in Stanford-University course material available on the web.[e] It is not immediately evident which engine condition this value corresponds to or whether or not this is a corrected value. It is assumed here that this mass flow rate is corrected using fan-face conditions or, equivalently, ambient conditions for a static engine and that the corrected value is also representative at the ADP. Under these assumptions, it follows that the corrected core mass flow rate at the HPC exit is 6 lbm/s (2.72 kg/s) for the CFM56-7B24 engine. This is a reasonable value for this class of turbofan engines and, in a sense, justifies the aforementioned assumptions. Consequently, this is the value used herein for the baseline engine. The corresponding value for the core mass flow rate when corrected using fan-face conditions is then 119.4 lbm/s (54.14 kg/s).

As can be seen in Appendix A, apart from a constant factor that depends only on the altitude, the ideal thrust can be expresses as a product of the core mass flow rate and a specific-thrust function. The specific thrust function depends on the flight Mach number, FPR, OPR, and BPR, as well as a parameter τ_λ which is related to the combustor exit total temperature. This total temperature also is not normally available in the open literature and consequently needs to be estimated. It was decided here to use 70 percent of the rule-of-thumb value for τ_λ, see Appendix Section A.8.8, which leads to $\tau_\lambda = 6.48$ and a combustor-exit, or turbine-inlet, total temperature, T_4, of 1418.37 K (2093 °F), at ADP. Using these values in the ideal-cycle analysis produces an ADP thrust of 5682.2 lbf (25.276 kN), which corresponds to 24082 lbf (101.122 kN) when corrected to SLS conditions. The thrust values are reasonable and leads to confidence in both the assumptions made as well as the ability of the ideal-cycle analysis to correctly identify trends. It is important to realize that the purpose of this report is not to present a detailed and highly accurate turbofan-engine model. Rather, the aim is to obtain a first estimate of the impact of the HyTEC parameter space on contributions to airport-community noise associated with the combustor by employing a simple, but meaningful, parametric turbofan analysis.

At this point, the parameters at the ADP for the hypothetical HyTEC-core turbofan engine need to be determined. With the ADP taken as the same as the baseline case, the OPR equals 58.3 as determined above. The remaining parameters are the FPR, τ_λ, and the BPR at the ADP. The FPR is here taken to be 1.35. The same 70-percent rule that was used for the baseline would here yield a T_4 above the plausible 2400–2700 °F target range for future high-performance gas generators. Consequently, T_4 at ADP is selected to be 1755.37 K (2700 °F). This aggressive value corresponds to $\tau_\lambda = 8.02$. The BPR must now be determined such that the thrust at the ADP equals the baseline-engine value. For a value of the the corrected mass flow rate at the compressor exit, w_{c3} ($\dot{m}_3^*$ in Appendices A and B), of 2.5 lbm/s (1.13 kg/s), Table 4 shows, in addition to some of the just described parameters, a resulting BPR of 13.4 and an ideal-cycle thrust-specific fuel consumption (TSFC) of 0.451 (lbm/h)/lbf [12.8 (g/s)/kN].

Table 4. Hypothetical HyTEC-Core Turbofan at ADP

TOC	10.668 km (35-thousand feet)
OPR	58.3
FPR	1.35
M_0	0.785
w_{c3}	2.5 lbm/s [1.13 kg/s]
BPR	13.4
TSFC	0.451 (lbm/h)/lbf [12.8 (g/s)/kN]

The corresponding ideal-cycle TSFC for the baseline case is 0.512 (lbm/h)/lbf [14.5 (g/s)/kN]. This value is somewhat better than a typical cruise TSFC value for the CFM56 turbofan,[f] which is as should be expected since no losses are accounted for in the present idealized parametric analysis. These ideal-cycle results indicates that up to an 11.9-percent improvement in fuel burn is theoretically possible, which is in line with KPP-1. Achieving this in practice represents significant turbo-fluid-mechanical, material, component- and overall-design challenges requiring sustained investments from industry and government stakeholders, however.

Figure 4(a) shows, apart from a multiplicative constant, the specific-thrust as a function of the BPR, with the other parameters fixed. The blue curve is for the baseline model, with the blue symbol indicating the baseline ADP value. The red curve corresponds to the new hypothetical small-core design, with the red symbol indicating the BPR leading to the same thrust as the baseline case. Note that the small-core corrected core mass flow rate at the HPC exit is 42 percent of the corresponding baseline value. However, the parametric analysis (see Appendix A) uses a core mass flow rate based on fan-face conditions. Recasting the requirement to the basis used in the ideal analysis means that the desired core mass flow rate is 68 percent of the baseline value. Thus, the specific thrust for the small-core design must be just under one-and-a-half times the baseline value. Figure 4(b) shows the propulsive efficiency as a function of the BPR, with the blue and red symbols indicating the baseline case and the new design.

[e] http://large.stanford.edu/courses/2011/ph240/nguyen1/docs/cfm-technical-data.pdf; last accessed 2021-09-16.
[f] https://en.wikipedia.org/wiki/CFM_International_CFM56; last accessed 2021-09-17.

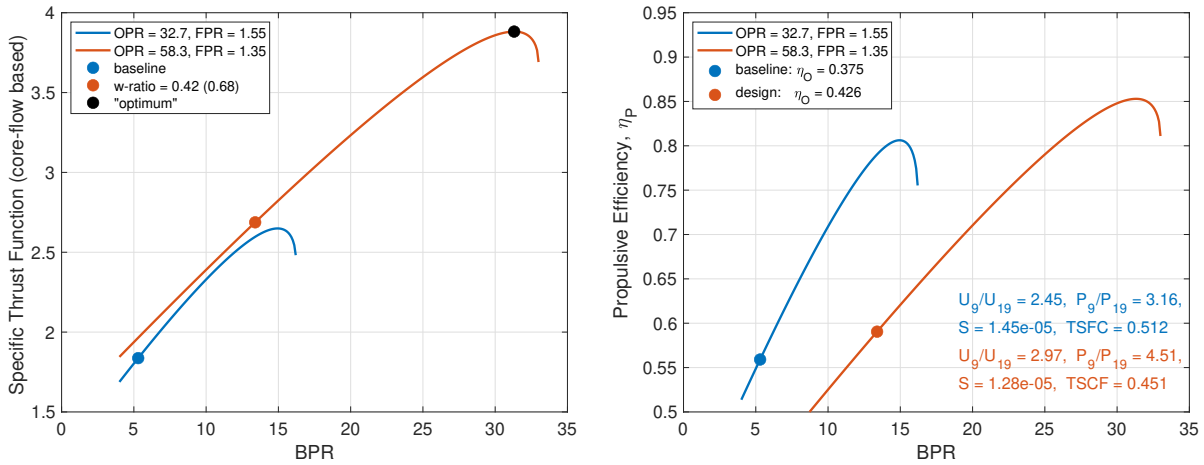

Figure 4. BPR Impact on Small-Core and Baseline Turbofans at ADP: (a) Specific Thrust Function; (b) Propulsive Efficiency

4 First Estimate of Acoustic Impact

An estimate of the effects of the HyTEC parameter space on combustor-noise levels can be obtained by utilizing the semi-empirical scaling law for combustor noise used in the ANOPP [5, 6] GECOR module. This model contains a formula for the total radiated acoustic power, with coefficients/constants determined, originally in the 1970s [7, 8], using extensive rig testing of isolated components and a large set of full-engine static-test data. In 1980, this method was adopted by the Society of Automotive Engineers International (SAE) as the SAE ARP876 [9] technical standard for the prediction of noise from conventional combustors installed in gas-turbine engines and it forms the kernel of the GECOR core-noise module. The GECOR module received extensions in the 1990s to cover a larger range of engine-thrust classes as well as other updates in the 2000s. See the SAE standard [9, Appendix D] for a background history of the SAE-method development and the reviews by Hultgren [10] and Tam et al. [11] for for discussions of combustor-noise modeling and prediction. The ANOPP-GECOR model is described in Appendix B.

Using the ANOPP-GECOR model to estimate the HyTEC impact on the radiated acoustic-power associated with the combustor is a tenuous exercise at best for two reasons, however. First, predictions using the original method were within 3–5 dB of the data for underlying individual engines [8]. Second, its applicability to emerging far-term designs is not fully known at present.[g] Nevertheless, Eq. (B 5) is used here, with the just mentioned caveats, to estimate the acoustic impact of the HyTEC parameter space.

The salient features of Eq. (B 5) for the emitted acoustic power, Π, can be expressed as

$$\Pi \propto \left(\frac{f h_{PR}}{\bar{c}_p}\right)^2 w_{c3} \left(\mathrm{OPR}\right)^{8/3.5} F_{TA}\,, \tag{1}$$

where constants and details that depend only on ambient conditions and the flight Mach number are ignored for simplicity. To incorporate flight-Mach-number effects, OPR is simply replaced by OCR in this formula. Note that Eq. (1) is not dimensionally correct. However, this formula clearly highlights the impact of the main potential design changes. Let's begin by examining the first factor on the right-hand side, which represents the square of the total temperature increase across the combustor. There, the heat release at constant pressure, h_{PR}, depends on the fuel used and is not likely to drastically change in the future since most alternate fuels are developed today to simply be 'drop-in-fuels' for Jet-A/A1. Even though the future combustor temperatures are expected to be higher, the average constant-pressure specific heat for the combustor, $\bar{c}_p$, will not change substantially. The open question, however, is how will the fuel-air ratio, f, be affected by the design changes. The hypothesis is made here that, for a given engine-operation condition, it will remain relatively unchanged. The validity of this seemingly reasonable assumption will have to be verified in future work, however. Keeping all this in mind, it can be concluded that the first factor on the right-hand-side of Eq. (1) is not significantly altered by transitioning into the HyTEC parameter space. Second

[g] However, there are indications that it might be applicable [12]

and third, the reduced core mass flow rate, w_{c3}, and increased OPR will decrease and increase the acoustic power, respectively. The fourth factor, F_{TA}, is a measure of the attenuation of the combustor noise as it passes through the turbine. Compared to modern turbines, future turbines are envisioned to have a reduced number of turbine stages, with each rotor having a lowered blade count (less solidity, but higher blade loading). This is likely to lessen the turbine attenuation of the combustor noise. Currently, there is no simple means of estimating this effect and it will simply be ignored for the purpose of this report. Consequently, it is the balance between the second and third factors in Eq. (1) that to a large extent determines the outcome.

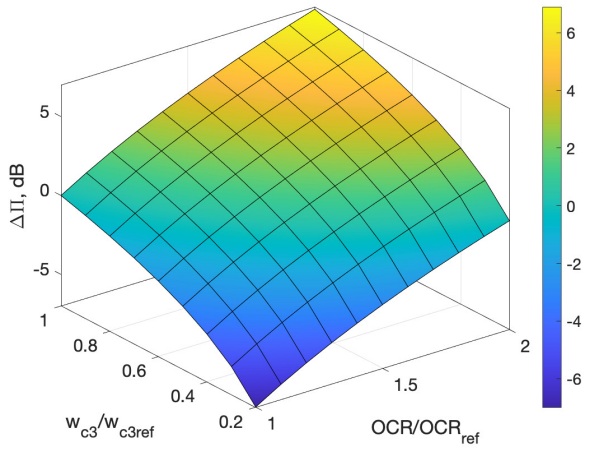

Figure 5. Impact on the Radiated Acoustic Power by Changes in the OCR and w_{c3}

Figure 5 shows the relative change in the radiated acoustic power in decibels (dB) as a function of relative changes in the OCR and corrected mass flow rate at the compressor exit. For a fixed flight Mach number, an OCR ratio is equivalent to an OPR ratio. A doubling of the OPR, which is characteristic of the current to far-term time frame, with an unchanged corrected mass flow rate, would lead to about a 7 dB increase in the combustor noise level. This doubling of the OPR has to be accompanied by a reduction in the corrected mass flow rate by a factor of $\frac{1}{5}$ in order for the combustor-noise level to essentially remain unchanged. This combination is actually typical [13] of early propulsion goals set for the far-term D8.5 double-bubble aircraft concept. However, in view of the HyTEC-Project performance parameter KPP-6, a 20-percent reduction is not considered realistic in the early 2030s EIS time frame.

Table 5. Acoustic-Power Change

OPR/OPR_{ref}	w_{c3}/w_{c3ref}	$\Delta\Pi$, dB
1.78	0.42	2.0
1.78	0.50	2.7
1.78	0.58	3.4

With the baseline as selected in this report, the HyTEC full- and minimum-success criteria would correspond to a 50- and 58-percent reduction in the corrected core mass flow rate, respectively. The ideal-cycle example in Section 3.2 has OPR and corrected core mass flow ratios of 1.78 and 0.42, respectively, with respect to the corresponding baseline values. Table 5 shows examples of estimated acoustic-power changes obtained using Eq. (1). It is concluded, that in the parameter regime desired by HyTEC project, the combustor-noise acoustic power would increase by about 3 dB. It is important to remember that noise certification criteria are not based on acoustic power, however, but that the measure used, EPNL, scales with the acoustic power (in particular when individual noise sources are considered).

Consequently, it can be concluded that at best the combustor-noise level will be doubled compared to what is observed today, but that a significant increase in the level is indeed also possible, particularly if the very aggressive reduction in corrected mass flow rate is not achieved. It is also important to point out that the noise level merely staying the same is not good enough.

5 Off-Design Acoustic Impact

It is of interest to also estimate the acoustic impact at turbofan off-design conditions. The ideal-cycle parametric model in Appendix A can be used for this purpose. It is important, however, to point out that the baseline-turbofan model does not actually represent the full performance of a CFM56 engine. The model represents an highly idealized turbofan engine with parameters chosen to reflect the characteristics of a CFM56 engine at ADP. It cannot be expected to yield highly accurate predictions at off-design conditions. However, it can illustrate trends as the engine-operation point moves away from the ADP. The same comments hold true for the design-model turbofan, with parameters taken to represent a high-power-density, small-core turbofan engine, in this report.

As can be seen in Appendix Section A.11, the HPT-IGV corrected mass flow rate and the HPT- and LPT-operation points all remain fixed at off-design operation, as long as the internal flowpaths remains choked at the assumed four locations. All other parameters are functions of only the corrected fan speed in this case. Figure 6 shows the turbine-inlet temperature parameter $\tau_\lambda/\tau_r = T_4/T_0$, the corrected temperature increase across the combustor, see Eq. (A 87), the compressor-exit corrected mass flow rate w_{c3}, and the OPR versus the corrected fan speed. The blue and red curves represent the baseline and design cases, respectively.

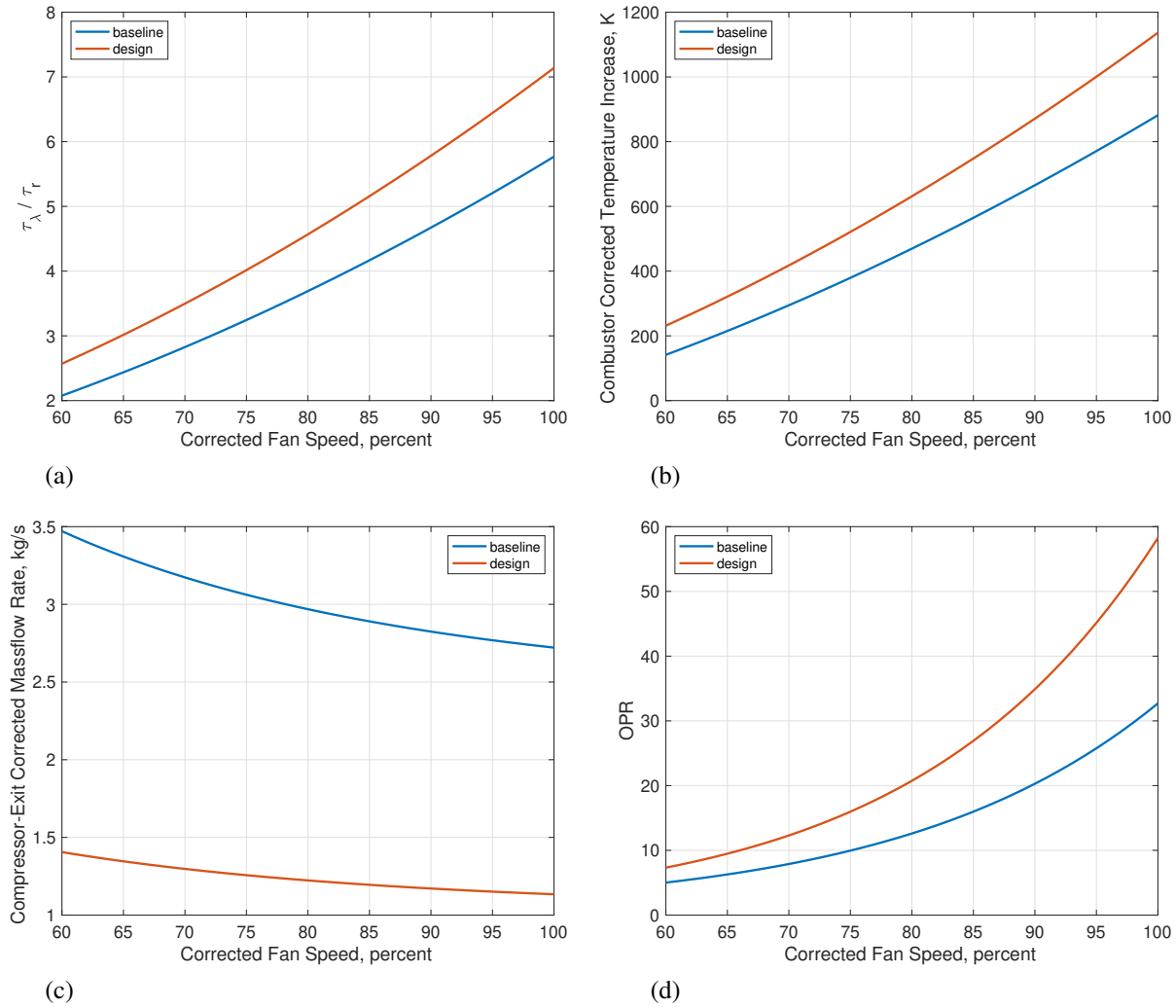

Figure 6. Ideal-Model Results Versus Corrected Fan Speed: (a) Turbine-Inlet Temperature Parameter; (b) Corrected Temperature Increase Across Combustor; (c) Compressor-Exit Corrected Mass Flow Rate; (d) Overall Pressure Ratio

The parameters shown in Fig. 6(b)–(c) and other turbofan-internal parameters, see Appendix Section A.11, do not depend on ambient conditions nor on the flight Mach number. However, the thrust, see Eq. (A 40), also depends on the flight Mach number because of the ram effect. If a flight profile is given, like the one required for noise certification, then the altitude and Mach number would be known as functions of time. If, in addition, any weight and drag differences resulting from changing the turbofans on the airframe in question from the baseline engine to the new-design one can be ignored, then the thrust requirement versus Mach number is known. That is, the new engine will need to deliver the same amount of thrust as the baseline turbofan at each flight-profile position. This requirement defines a relationship between the corrected fan speeds of the two aeroengines at off-design operation. This is the course of action that will ultimately have to be employed when estimating changes to the EPNL. The implementation of this procedure for a general flight profile is beyond the scope of the present report, however. It is left for future work.

The off-design acoustic impact can readily be estimated for a static-engine test,[h] however. Figure 7(a) shows the corrected thrust at static-engine conditions for the two idealized (baseline and design) models. Although both models predict identical corrected thrust at the ADP, at static conditions they do not because of the absence of the ram effect. Also note that the simple idealized models ultimately fail to predict the corrected thrust as the corrected fan speed is reduced. This is not a great concern, however, since the choked flow assumptions can not be expected to continue to hold as the corrected fan speed is reduced. Consequently, a more complicated model would have to be used for lower corrected fan speeds. The curves here are plotted for a corrected-fan-speed range where both turbofan models yield corrected-thrust results. The ideal models used here are expected to describe trends reasonably well in the upper range of the considered corrected fan speeds, but with reduced accuracy in the lower range.

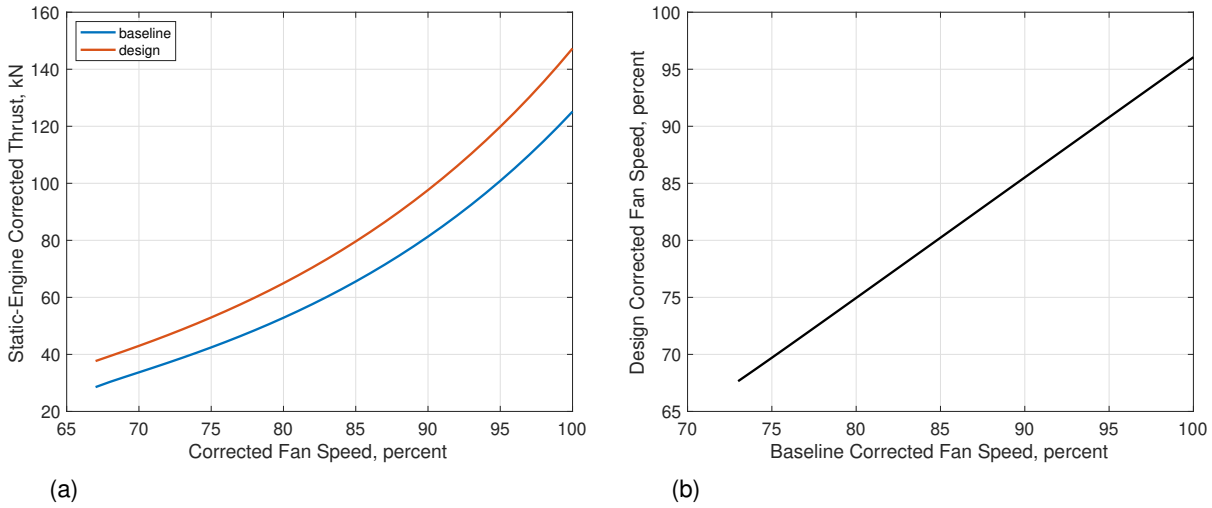

Figure 7. Static-Engine Results: (a) Corrected Thrust; (b) New-Design Corrected Fan Speed Versus Baseline Corrected Fan Speed

A reasonable procedure to use for estimating the acoustic impact of a design change is to compare results for the new-design and baseline engines at given amounts of thrust. The individual engine operating points are selected such that each engine generates the same amount of thrust, i.e., their relative corrected fan speeds are not the same. Figure 7(b) shows the so determined new-design corrected fan speed versus the baseline corrected fan speed under the static-engine conditions. Maybe somewhat surprisingly, a linear dependency between the corrected speeds is evident. Figure 8 shows the same quantities as Fig. 6, but now under the constraint that both engines produce the same thrust. It is clear from these results that the lower corrected fan speed needed for the small-core design will counteract other effects on the combustor-noise level due to the design change. It is instructive to also illustrate these ideal-cycle results in terms of ratios of the new-design to baseline values. This is done in Fig. 9.

[h] A static-engine test can be thought of as a flight profile with zero Mach number at zero altitude.

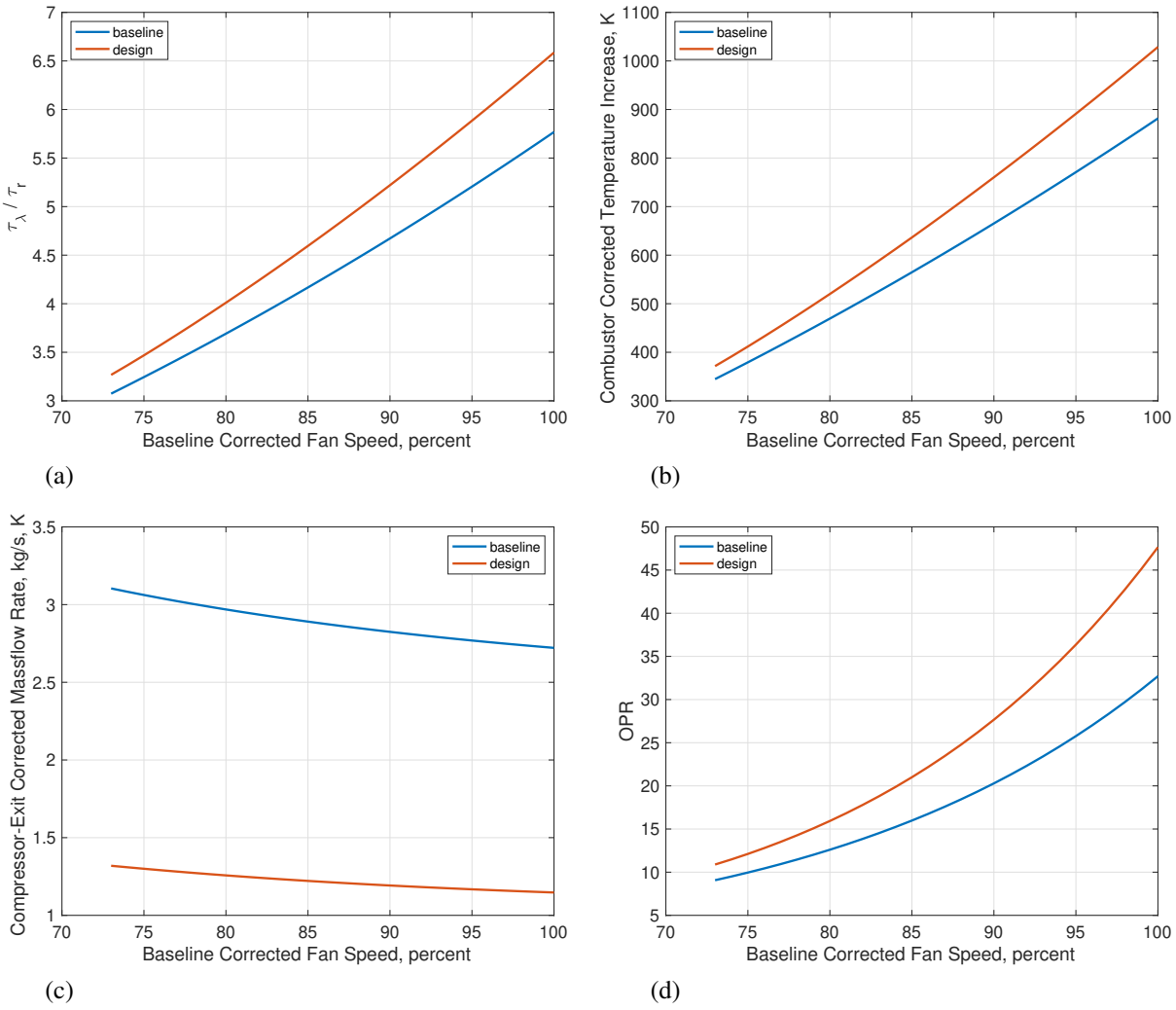

Figure 8. Equal-Thrust Results Versus Corrected Fan Speed at Static-Engine Conditions: (a) Turbine-Inlet Temperature Parameter; (b) Corrected Temperature Increase Across Combustor; (c) Compressor-Exit Corrected Mass Flow Rate; (d) Overall Pressure Ratio

Figure 9(a) as well as Fig. 8(a) show, as expected, that the HPC-IGV temperature T_4 is higher for the new-design turbofan. The new-design-to-baseline T_4 ratio decreases as the corrected fan speed is lowered during static-engine conditions. Figure 9(b) shows that the total temperature difference across the combustor, ΔT, for the new-design is larger when compared to the baseline value. This increase varies monotonically from about 8 percent to 17 percent with the corrected fan speed, i.e., the static-engine thrust. This, by itself, would correspond to an increase in the combustor-noise acoustic power of about 0.7–1.4 dB. Figure 9(c) shows that the ratio of the compressor-exit corrrected mass flow rates stays relatively constant. This ratio starts out at about 0.425 at the lowest shown value of the corrected fan speed shown and monotonically decreases to about 0.422 at full speed. This implies a reduction of the acoustic power ranging from -3.72 dB to -3.75 dB, basically overall about -4 dB. Figure 9(d) shows essentially a linear increase in the new-design-to-baseline OPR ratio for the static-engine situation considered here. The impact on the combustor-noise acoustic power from the OPR effect is estimated to be an increase of about 1.8 dB to 3.7 dB.

The combined impact of these effects on the combustor-noise total emitted acoustic power is shown in Fig. 10 as the purple curve. The yellow curve in Fig. 10 represents a static-engine test where the corrected fan speeds, relative to their ADP values, are matched rather than the thrust produced by the engines. The quite drastic change between the situations represented by these curves is simply due to the fact that the hypothetical new-design turbofan produces the required static thrust at a lower corrected fan speed percentage than the hypothetical baseline engine, see Fig. 7(b).

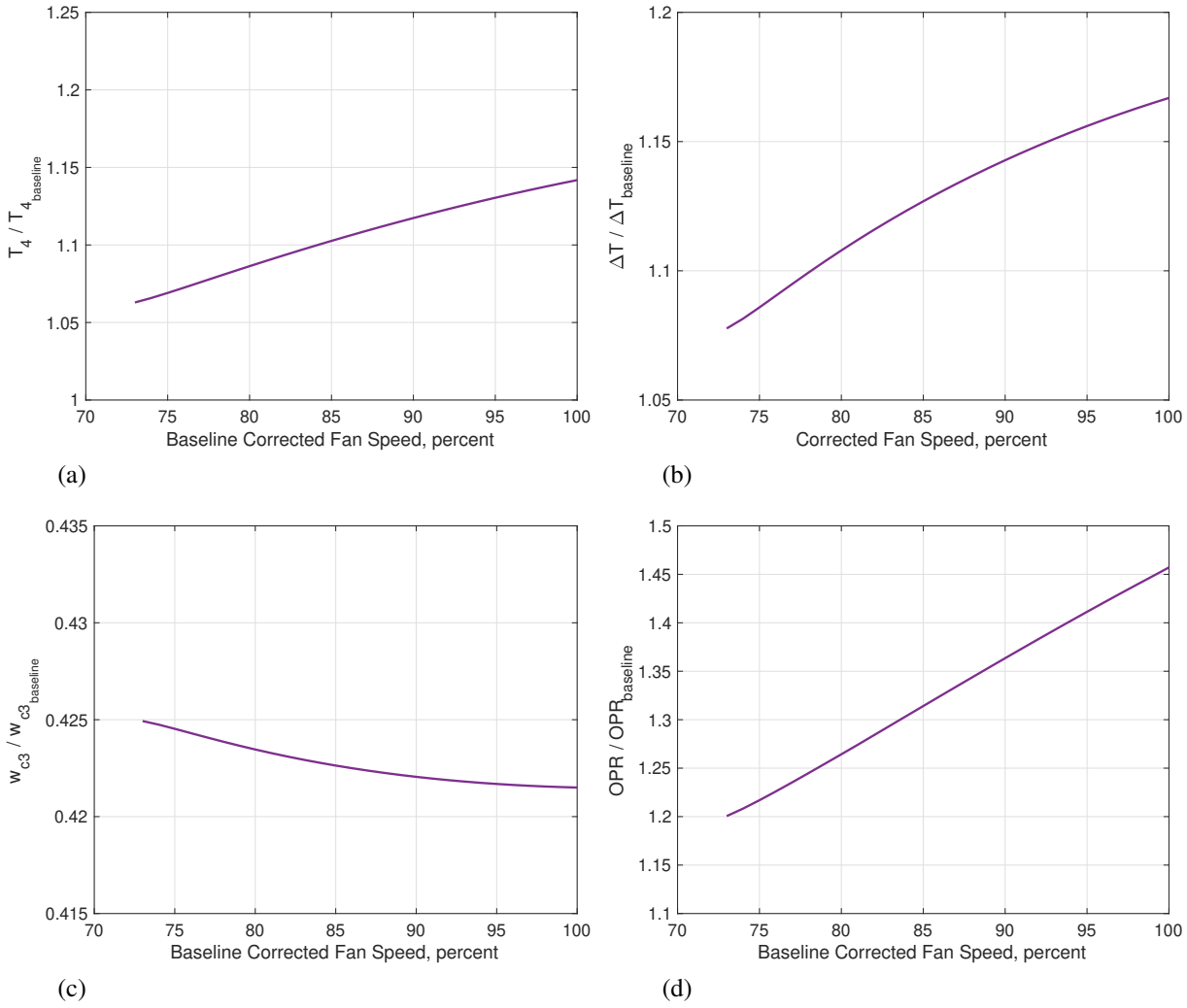

Figure 9. Equal-Thrust Parameter Ratios Versus Corrected Fan Speed at Static-Engine Conditions: (a) Turbine-Inlet Temperature; (b) Temperature Increase Across Combustor; (c) Compressor-Exit Corrected Mass Flow Rate; (d) Overall Pressure Ratio

Consequently, the lower throttle setting needed for thrust matching reduces the total temperature increase across the combustor, the compressor-exit corrected mass flow rate, as well as the OPR—each of which reduces the combustor-noise acoustic power. Furthermore, the difference between the 100-percent corrected fan speed static result (gold curve) in Fig. 10 and the corresponding ADP estimate in Fig. 5 is explained by the fact that for this particular example the difference in the total-temperature increase across the combustor cannot be ignored as was assumed in Section 4.

The purple-curve result in Fig. 10 indicating a combustor-noise reduction compared to the baseline case at lower thrust values (lower baseline fan speeds) has to be interpreted with some caution. Namely, the choked-flow ideal-cycle assumptions will start to be violated at some point as the thrust is reduced. Nevertheless, the ideal-cycle parametric static-engine study carried out here points to the possibility that a high-power-density, small-core turbofan, being generally more efficient than its baseline counter part, could have less of a combustor-noise issue at, say, approach conditions than at the ADP conditions. A more complete cycle analysis is indeed needed to underpin this possible scenario.

A first step in this regard would be to introduce a different, but constant, value for the ratio of specific heats at constant pressure in the post-combustor flowpath and to introduce component and shaft efficiencies into the ideal-cycle analysis. It is the author's opinion that reasonable assumptions for efficiencies can be made for the basline-turbofan model based on general-community knowledge, but that it is not clear what would be reasonable assumtions for the

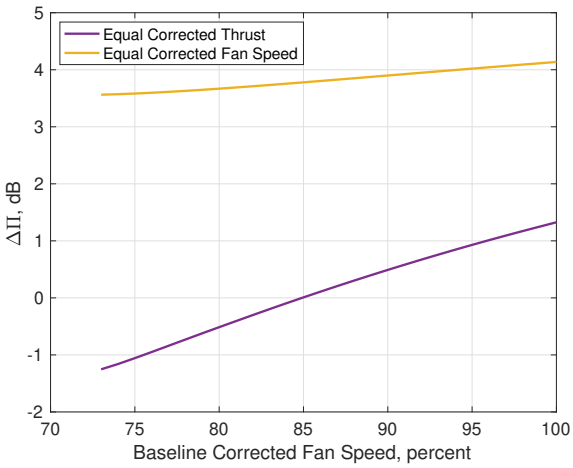

Figure 10. Impact on the Radiated Acoustic Power at Static-Engine Conditions

rotating components in the emerging small-core design space. In addition, some (maybe all) of the choked-flow assumptions would need to be relaxed. Consequently, detailed engine-deck studies such as those provided by the NPSS are ultimately needed.

6 Summary and Conclusions

Ideal-cycle parametric studies are carried out for two hypothetical turbofan engines. The design parameters for the first, the baseline, are chosen such that the model corresponds to a CFM56-7B engine at it aerodynamical design point, based only on open information. The second model is for a high-power-density, small-core turbofan. Its design parameters are chosen to mimic a desired end result for the development effort carried out under the NASA HyTEC Project.

The purpose of this study is not to perform a detailed, extensive, or highly accurate turbofan design study. Rather, the aim is to generate reasonable input parameters, and a procedure, for an initial assessment of the impact of this desired turbofan design trend towards compact cores on the aeroacoustic noise associated with sources in the combustor. Consequently, the simplest possible turbofan-model assumptions are employed. Furthermore, no design optimization is carried out for the new-design turbofan—it simply represents a model case that satisfies the HyTEC goals.

The formula for the total radiated acoustic power from sources in the combustor, used in the NASA Aircraft Noise Prediction Program, is recast to utilize the parameters generated by the ideal-cycle-turbofan models. General scaling results obtained by examining this formula under one simplifying assumption are presented. It is concluded from this 'global' assessment that the combustor-noise acoustic power level is likely to double (3 dB increase) for turbofans in the HyTEC design space compared to modern turbofans of a similar thrust class.

Next, a static-engine-test scenario is examined. An engine comparison can be carried out utilizing at least two obvious criteria. The first involves both turbofans having equal fractional corrected fan speed, where a 100-percent setting represents the aerodynamical-design-point speed. The second is based on both engines generating the same amount of thrust. Comparisons are carried out using both criteria. Both modeled test scenarios show that the simplifying assumption used for the the 'global' estimate, i.e., that the total-temperature increase across the combustor is about equal for the two engines, leads to an underestimation of the acoustic-power change. In the static-test scenario with matched fractional corrected fan speeds, the comparison shows an increase in the emitted combustor-noise total acoustic power of about 3.5–4 dB, with the larger value at top speed.

In the matched-thrust case, the new-design turbofan model indicates that a lower fractional corrected fan speed is needed to generate the same amount of thrust as the baseline-engine model. This leads to an overall reduction of the of the predicted acoustic-power difference between the engines, even leading to a low-speed range where the level is decreased by as much as about 1 dB. At maximum speed (based on the baseline turbofan), the acoustic-power increase is here just about 1 dB. The higher 'efficiency' of the new-design turbofan under static-test conditions means that in this case the acoustic-power level essentially can be considered as unchanged.

There are at least two caveats in regards to these static-engine-test conclusions. First, the simple idealized model used to predict the engine performance will start to lose its predictive capability as the corrected fan speed is decreased. This is so because, at some point, the underlying assumption of choked flow at four different locations of the engine-internal flow paths will start to fail one by one. However, there is no obvious indication in the results to detect this expected reduction of accuracy or violation of assumptions for the model(s) used. Consequently, not too much emphasis should be put on results at the lower speeds. Nevertheless, the static-engine results do indicate that during takeoff operations (which include the sideline and flyover noise certification points), the radiated combustor-noise acoustic-power level essentially could remain unchanged.

Second, the thrust versus engine corrected fan speed relationship will be different due to ram effects during flight. Hence, the static-engine acoustic-power results may not directly carry over to an in-flight situation. In order to sort out this issue, future work is planned to 'fly' these turbofan-engine models using identical prescribed flight profiles. The flight profile will provide altitude, flight Mach number, and required thrust as functions of time. This will enable the comparison for these two hypothetical turbofans of the combustor-noise effective-perceived-noise levels as used in noise certification procedures.

Improvements to the models, that incorporate a bit more physics (component efficiencies and improved thermodynamic constants) can also be made, but ultimately engine decks based on results obtained using the Numerical Propulsion System Simulator are needed, for a more accurate assessment.

Based on the results in this interim assessment, it can be concluded that at best the combustor-noise level could be similar to what is observed today, but that a significant increase in the level is indeed also possible, particularly if the very aggressive reduction in corrected mass flow rate is not achieved. In this respect, it is important to realize that merely staying the same is not good enough since that would ultimately limit the effectiveness of noise mitigation technologies applied to other propulsion-noise sources.

The challenges in achieving a high-power-density, small-core turbofan aeroengine in practice are indeed significant. The ultimate success requires persistent turbo-fluid-mechanical, material, component- and overall-design research efforts and investments from all stakeholders. Core-noise research needs to be a part of this effort.

APPENDICES

A Ideal-Turbofan Parametric Analysis

Parametric cycle analyses of idealized aeroengines, even though highly simplified, lead to an understanding of major engine-design parameters and their interplay. Gas-turbine textbooks, e.g. Kerrebrock [14] and Mattingly [15], usually give exhaustive presentations on this subject. For convenience, pertinent details of the idealized cycle analysis for a turbofan, as well as some supporting concepts, are summarized below.

A.1 *Turbofan Engine Performance Stations*

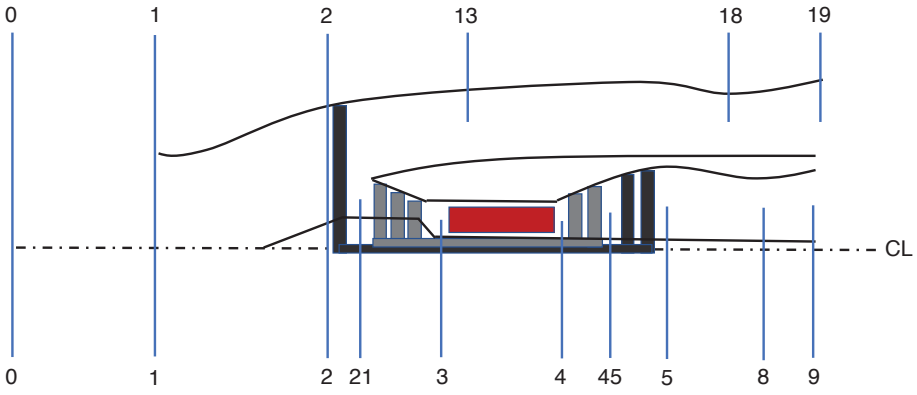

Figure A 1. Turbofan performance-station identification following SAE ARP755A [16]

Figure A 1 shows the engine stations needed for a mean-line performance analysis of a typical dual-spool turbofan engine, with a separate-flow-path nozzle. The performance stations are numbered in accordance with Society of Automotive Engineers International (SAE) Aerospace Recommended Practices ARP775A [16]. The stations are as follows:

0: free stream conditions
1: engine inlet
2: fan front face
21: high-pressure compressor front face
3: high-pressure compressor exit plane (compressor diffuser exit plane)/combustor inlet
4: combustor exit/high-pressure turbine inlet-guide-vane front face
41: high-pressure turbine inlet-guide-vane exit plane (not shown)
45: high-pressure-turbine exit plane/low-pressure-turbine front face
5: low-pressure-turbine exit plane
7: core-nozzle inlet (not shown/coincides with station 5)
8: core-nozzle throat
9: core-nozzle exit plane
13: fan exit
17: fan-nozzle inlet (not shown/coincides with station 13)
18: fan-nozzle throat
19: fan-nozzle exit

The low-pressure (LP) spool (dark gray) consists of the fan, the low-pressure turbine (LPT), and the connecting shaft. The LP spool shaft speed is denoted by N_1, or N_{L}. The high-pressure (HP) spool (light gray) consists of the high-pressure compressor (HPC), the high-pressure turbine (HPT), and the connecting shaft. The HP spool shaft speed is denoted by N_2, or N_{H}. The combustor location is indicated by the dark red rectangle in the figure.

A.2 *Basic Notation*

Following recommended practice [16], static thermodynamic properties (state variables) will have the additional subscript 's' added ahead of the station identifier, eg. $T_{\mathrm{s}2}$ denotes the static temperature at station 2, whereas T_2 is the corresponding total (or stagnation) temperature. The reverse choice of adding a subscript prefix of 't' for total thermodynamic properties and interpreting thermodynamic properties with non-prefixed subscripts as static would also have been a logical notation with 'cleaner' formulas for thermodynamic properties. However, the 'traditional' turbomachinery choice followed herein leads to formulas with simpler notation for the performance analysis, which out weights the resulting increase in complexity of thermodynamic-relationship notation.

A.3 *Thermodynamic Relationships and Properties*

A.3.1 *Non-Reacting Calorically Perfect Gas* Except in the reaction zone(s) in the combustor, the flow is taken to be that of a calorically perfect gas. That is, the working fluid is described by the ideal gas law

$$P_{\mathrm{s}} = \rho_{\mathrm{s}} R T_{\mathrm{s}}\,, \tag{A 1}$$

where P_{s}, T_{s}, and ρ_{s}, are the static (or state variables) pressure, temperature, and, density, respectively, R is the gas constant [287.058 J/(kg K) for dry air]; and the equation of state

$$h_{\mathrm{s}} = c_p T_{\mathrm{s}}\,, \tag{A 2}$$

where h_{s} is the specific enthalpy and the specific heat at constant pressure, c_p, is a constant. Since c_p is constant, the specific heat at constant volume, $c_v = c_p - R$, and the ratio of specific heats, $\gamma = c_p/c_v$, are also both constant.

The specific entropy, s, is given by

$$s(T_{\mathrm{s}}, P_{\mathrm{s}}) = s^{(\mathrm{o})} + c_p \ln(T_{\mathrm{s}}/T^{(\mathrm{o})}) - R\ln(P_{\mathrm{s}}/P^{(\mathrm{o})})\,, \tag{A 3}$$

where the superscript 'o' indicates values at the thermodynamic reference state (101.325 kPa, 298.15 K).

Because of the large temperature changes experienced by the mean-line flow in turbomachinery, this simplified approach in reality should not be uniformly implemented throughout the turbofan. However, it can be applied on a local basis for most of the turbofan components without too much loss of accuracy in the analysis [14, 15]. In general, other effects, ignored in a typical mean-line analysis, can be expected to have a greater influence on the results for a particular component than whether the specific heats are assumed constant or not. As suggested by Kerrebrock [14] and Mattingly [15], among others, a useful approach is to use two different sets of values for the ratio of specific heats and the specific heat at constant pressure. One set is used in the flow path downstream of the combustor and the other set is used everywhere else, except in the combustor which is analyzed separately. However, an ideal-cycle parametric study assumes c_p (and consequently also γ) as having a constant value throughout the aeroengine.

A.3.2 ***Total or Stagnation Properties*** A total, or stagnation, property is defined as the value of a certain property resulting from the flow being brought to rest through an isentropic, i.e. both adiabatic and reversible, process, without any involvement of external work. The total specific enthalpy, h, is the sum of the static specific enthalpy and specific kinetic energy, which for a calorically perfect gas is

$$h = h_\mathrm{s} + \tfrac{1}{2}U^2 = h(T_\mathrm{s}) + \tfrac{1}{2}\gamma R T_\mathrm{s} M^2 = c_p T_\mathrm{s}\left[1 + \tfrac{1}{2}(\gamma-1)M^2\right], \tag{A 4}$$

where U is the mean-line velocity, $M = U/a$ is the Mach number, with $a = \sqrt{\gamma R T_\mathrm{s}}$ being the local speed of sound. The total temperature T can be introduced as

$$T = T_\mathrm{s}\left[1 + \tfrac{1}{2}(\gamma-1)M^2\right], \tag{A 5}$$

i.e., T is the temperature that when inserted into (A 2) yields the same value as (A 4) evaluated for the corresponding static temperature T_s and Mach number M. Thus, the total temperature $T = T(T_\mathrm{s}, M)$ is simply the isentropic stagnation temperature, i.e. the temperature achievable by converting all the kinetic energy of a flow to internal energy.

Since a stagnation condition, by definition, is a thermodynamic state, Eq. (A 3) also holds true when the static variables on the right-hand side are replaced by the corresponding total variables, i. e.,

$$s(T,P) = s^{(\mathrm{o})} + c_p \ln(T/T^{(\mathrm{o})}) - R\ln(P/P^{(\mathrm{o})}), \tag{A 6}$$

where P is the total, or isentropic stagnation, pressure. By specification, the stagnation-state and the flowing-gas entropies are identical, i.e.,

$$s(T,P) = s(T_\mathrm{s}, P_\mathrm{s}). \tag{A 7}$$

In view of Eqs. (A 3),(A 6), and (A 7), the total pressure is given by

$$P = P_\mathrm{s}\,(T/T_\mathrm{s})^{\gamma/(\gamma-1)} = P_\mathrm{s}\left[1 + \tfrac{1}{2}(\gamma-1)M^2\right]^{\gamma/(\gamma-1)}. \tag{A 8}$$

Since the stagnation state also must satisfy the ideal gas law Eq. (A 1), it follows that the total density, ρ, is given by

$$\rho = \frac{P}{RT} = \rho_\mathrm{s}\left[1 + \tfrac{1}{2}(\gamma-1)M^2\right]^{1/(\gamma-1)}. \tag{A 9}$$

A.4 *Conservation Laws*

A.4.1 ***Conservation of Mass*** The flow of air entering the engine is divided into the engine core and the fan-bypass duct, i.e.,

$$\dot{m}_\mathrm{I} = \dot{m}_\mathrm{C} + \dot{m}_\mathrm{F} = (1+\alpha)\dot{m}, \tag{A 10a}$$

where $\dot{m}_\mathrm{I}$, $\dot{m}_\mathrm{C} \equiv \dot{m}$, and $\dot{m}_\mathrm{F} = \alpha\dot{m}$ are the overall (inlet), core, and fan-duct mass flow rates, respectively, $\alpha \equiv \dot{m}_\mathrm{F}/\dot{m}_\mathrm{C}$ is the engine bypass ratio (BPR), and $\dot{m}$ is a simplified notation for the mass flow rate entering the core. The subscript 'C' will only be used when needed for clarity. Furthermore, any bleed flows in the core are ignored in the idealized situation considered here.

The ratio of the fuel and air mass flow rates entering into the combustor, which is commonly referred to as the fuel-air ratio (FAR), is denoted by f. The mass flow rate through the turbine and core nozzle, $\dot{m}_\mathrm{T}$, is then given by

$$\dot{m}_\mathrm{T} = (1+f)\dot{m}. \tag{A 10b}$$

Note that the fuel-air ratio is normally a rather small number—for the Olefin family of hydrocarbon fuels, its stochiometric value is about 0.0676. Consequently, f can be neglected, when compared to $O(1)$ quantities, in expressions such as Eq. (A 10b). For the core gas flow downstream of the combustor, the effects on the thermodynamical properties from the small composition change due to the presence of combustion products can also be ignored in an idealized analysis since $f << 1$.

A.4.2 ***Conservation of Momentum*** The conservation of momentum in the streamwise direction shows that the thrust, F, is given by

$$F = \dot{m}\left[\alpha U_{19} + (1+f)U_9 - (1+\alpha)U_0\right], \tag{A 11}$$

where U_{n} is the mean-line velocity at station 'n'. It has been assumed in the derivation of Eq. (A 11) that the static pressures at the core- and fan-nozzle exits, $P_{\mathrm{s}9}$ and $P_{\mathrm{s}19}$, both equal the free-stream static pressure, $P_{\mathrm{s}0}$.

A.4.3 ***Conservation of Energy*** The conservation of energy for a control volume reads

$$\int_S \rho_{\mathrm{s}} h \vec{U} \cdot \mathrm{d}\vec{S} = \dot{Q} + \dot{W}, \tag{A 12}$$

where the left-hand side represents the net flux of total enthalpy leaving the control volume, and $\dot{Q}$ and $\dot{W}$ are the rates at which heat is added to and work is performed on the control volume.

A.5 *Control-Volume or Stream-Tube Analysis*

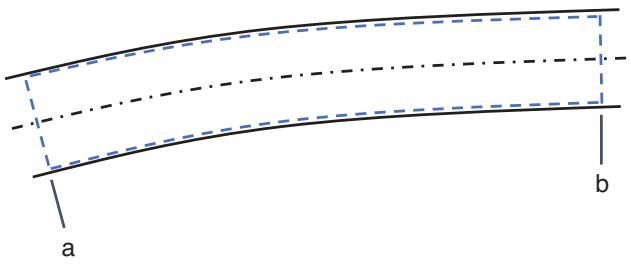

Figure A 2. Control volume inside a section of a duct or stream tube

Consider steady flow through the control volume indicated by the blue dashed lines in Fig. A 2. The solid black lines represents the boundaries of a stream tube (or duct walls)—the underlying feature is that there is no flow across these boundaries. Conservation of mass then implies that

$$\dot{m}_{\mathrm{b}} = \dot{m}_{\mathrm{a}}, \tag{A 13}$$

i.e., the mass flow rate is constant.

A.5.1 ***Adiabatic Flow Without Work Performed*** If there is no heat added to or no work performed on the flow depicted in Fig. A 2, then Eqs. (A 12) and (A 13) imply that

$$h_{\mathrm{b}} = h_{\mathrm{a}}, \tag{A 14}$$

i.e., the total enthalpy h is constant. The total enthalpy depends on the static temperature T_{s} and the Mach number M or alternatively only on the total temperature T. Consequently, in view of the second alternative, *the total temperature T is constant for an adiabatic flow with no mechanical work addition/extraction*, i.e.

$$T_{\mathrm{b}} = T_{\mathrm{a}}. \tag{A 15}$$

It is important to realize that (A 15) holds true even if there are losses inside the control volume—the only requirement is that no work or heat transfer take place. The effect of losses is simply that kinetic energy is converted to internal energy, i.e., the static temperature is increased due to viscous friction, but the total temperature remains unchanged.

Equation (A 6), applied to the situation shown in Fig. A 2, implies that

$$\frac{P_\mathrm{b}}{P_\mathrm{a}} = \exp\left(-\Delta s/R\right) \leq 1\,, \tag{A 16}$$

since the entropy change between the two stations $\Delta s \equiv s_\mathrm{b} - s_\mathrm{a} \geq 0$, i.e., losses reduce the total pressure. Equation (A 16) shows that *the total pressure P is a constant for loss-less adiabatic flow when work is not performed.*

A.5.2 ***Isentropic Compression and Expansion*** If isentropic compression or expansion occurs between stations 'a' and 'b' in Fig. A 2, Eqs. (A 3) and (A 6) show that, for a calorically perfect gas,

$$\frac{P_\mathrm{sb}}{P_\mathrm{sa}} = \left(\frac{T_\mathrm{sb}}{T_\mathrm{sa}}\right)^{\frac{\gamma}{\gamma-1}}\,, \tag{A 17}$$

$$\frac{P_\mathrm{b}}{P_\mathrm{a}} = \left(\frac{T_\mathrm{b}}{T_\mathrm{a}}\right)^{\frac{\gamma}{\gamma-1}}\,, \tag{A 18}$$

respectively, i.e., the isentropic-process pressure-temperature relationships are analogous (identical form) for the static and the total variables. Again, Eqs. (A 15) and (A 18) imply that *the total pressure P is constant for an isentropic flow with no mechanical work addition/extraction*.

A.6 *Turbofan Component Performance Characterization*

A.6.1 ***Total-Pressure and Total-Temperature Ratios*** As is customary [14, 15], the operational state of a turbofan component is described by the actual total-pressure and total-temperature ratios across the component, i.e.,

$$\pi = P_\mathrm{b}/P_\mathrm{a}\,, \tag{A 19a}$$

$$\tau = T_\mathrm{b}/T_\mathrm{a}\,, \tag{A 19b}$$

where stations 'a' and 'b' represent inlet and exit conditions, respectively (eg. Fig. A 2). A subscript denoting the component is usually added when needed for clarity. Here, the subscripts 'd', 'f', 'c', 'b', 't', 'n', and 'F' denote the inlet, fan, fan+compressor, combustor (burner), turbine, core nozzle, and fan nozzle, respectively. It is customary to use the single symbol $\pi_c = P_3/P_2$ for the overall pressure ratio (OPR) experienced by the core stream across the fan and compressor (the full compression chain), rather than using the product of two total-pressure ratios, since this leads to a simpler notation. Furthermore, following Mattingly [15],

$$\pi_r = P_0/P_\mathrm{s0} = \tau_r^{\gamma/(\gamma-1)}\,, \tag{A 20a}$$

$$\tau_r = T_0/T_\mathrm{s0} = 1 + \tfrac{1}{2}(\gamma-1)M_0^2\,, \tag{A 20b}$$

are introduced to describe the freestream total-to-static pressure and temperature ratios. Recall that the static temperature and static pressure are thermodynamic state variables, which are independent of the frame of reference (stationary or moving). Consequently, the static temperature and static pressure at turbofan station '0' are given by the ambient atmospheric conditions. The freestream Mach number, M_0, is determined by the forward speed of the engine/aircraft and the ambient conditions. For a static engine test $M_0 = 0$.

A.6.2 ***Efficiency*** The isentropic efficiency of a component is defined as

$$\eta = \frac{h_\mathrm{bi} - h_\mathrm{a}}{h_\mathrm{b} - h_\mathrm{a}} = \frac{\pi^{(\gamma-1)/\gamma} - 1}{\tau - 1}\,, \tag{A 21a}$$

or

$$\eta = \frac{h_\mathrm{b} - h_\mathrm{a}}{h_\mathrm{bi} - h_\mathrm{a}} = \frac{\tau - 1}{\pi^{(\gamma-1)/\gamma} - 1}\,, \tag{A 21b}$$

depending on what type of component is being considered. The subscript 'i' indicates the isentropic (ideal) value of the total enthalpy at the exit corresponding to the component actual total pressure ratio π. For compressors, the actual total-entropy change is always larger than the isentropic value and hence Eq. (A 21a) applies. Equation (A 21b) corresponds to turbines for which the actual total-entropy change is always less than the isentropic value. It follows that a component operational condition can be characterized by (π, η) as an alternative to (π, τ)—note that $\eta = \eta(\pi, \tau)$, however. The isentropic efficiency is a measure on how close an actual process is to being isentropic. There are other common efficiency measures, such as polytropic efficiency and velocity and mass flow rate coefficients for nozzles. For diffusers, including the inlet, the total-pressure ratio π_d is a common performance metric. These other measures will not be discussed here, however. It is sufficient to point out that for the present purpose of performing an ideal cycle analysis,

$$\eta = 1 \tag{A 22}$$

for all components where isentropic efficiency is an appropriate component performance criterion. Except for the combustor, the ideal assumption, Eq. (A 22), implies that the total-temperature ratio across a component is directly known in terms of the corresponding total-pressure ratio, i.e. $\tau = \pi^{(\gamma-1)/\gamma}$.

A.7 *Parameter Characterization*

Following Mattingly [15], the cycle parameters are characterized into four different categories, namely: flight condition, design limitation, performance of 'non-work' components, and design parameters.

A.7.1 ***Flight Condition*** The flight condition is uniquely defined by specifying the altitude and the aircraft Mach number, M_0. The ambient static conditions $P_{\mathrm{s}0}$ and $T_{\mathrm{s}0}$, as well as the speed of sound a_0, are then obtained from the 1976 U.S. Standard Atmosphere [17]. Note that the 1976 U.S. Standard Atmosphere assumes a constant value of $\gamma = 1.4$, which corresponds to a constant value of $c_p = 1.0047$ kJ/(kg K). Alternatively, the ambient conditions $P_{\mathrm{s}0}$ and $T_{\mathrm{s}0}$, and the thermodynamical property c_p or γ could simply be specified in addition to the flight Mach number, M_0.

A.7.2 ***Design Limitation*** The main design limitation is set by material properties, namely there is a maximum temperature that the turbine can tolerate without experiencing a reduced service life. The combustor-exit total temperature, T_4 is the corresponding design-limitation parameter. Some authors, eg. Mattingly [15], introduce the parameter

$$\tau_\lambda \equiv \frac{h_4}{h_{\mathrm{s}0}} = \frac{T_4}{T_{\mathrm{s}0}}\,, \tag{A 23}$$

where the last step is strictly speaking only valid under the ideal-cycle assumptions, as a representative parameter for this design limit.

A.7.3 ***Component Performance*** The next set of parameters are associated with components, such as inlet and nozzles, were no work is added or extracted, and the combustor. In the ideal-cycle analysis, their total-pressure ratios,

$$\pi_\mathrm{d} = \pi_\mathrm{b} = \pi_\mathrm{n} = \pi_\mathrm{F} = 1\,, \tag{A 24}$$

are considered as given performance parameters.

A.7.4 ***Design Parameters*** The fan and compressor total-pressure ratios, core mass flow rate, and bypass ratio, π_f, π_c, $\dot{m}$, and α are considered as parameters available to the designer for achieving a desired performance. The turbine total-pressure ratio, π_t, is uniquely determined by the compressor and fan power requirements. Alternatively, the total-temperature ratios τ_f or τ_c can each replace its corresponding total-pressure ratio as a design parameter if so desired.

A.8 *Cycle Analysis*

By ignoring impact of the small fuel flow rate, the thrust equation, Eq. (A 11), can be written as

$$F = a_0 \dot{m} \left[M_9 \frac{a_9}{a_0} - M_0 + \alpha (M_{19} \frac{a_{19}}{a_0} - M_0) \right] . \tag{A 25}$$

The thrust contributions from the core and fan flow now need to be related to the design parameters in order to evaluate the impact of the latter on the total thrust.

A.8.1 ***Core Flow*** The dependencies on the design parameters for the quantities M_9 and U_9/a_0 are obtained as follows: First, the energy balance for the combustor, to the required accuracy, yields

$$T_3 + f h_{PR}/c_p = T_4 \, , \tag{A 26}$$

where h_{PR} is the specific heating value of combustion for the fuel (typically 42.8 MJ/kg for jet fuel). Equation (A 26) can be manipulated to obtain the two expressions

$$\frac{f h_{PR}}{c_p T_{s0}} = (\tau_b - 1) \tau_r \tau_c \, , \tag{A 27a}$$

$$\frac{f h_{PR}}{c_p T_{s0}} = \tau_\lambda - \tau_r \tau_c \, . \tag{A 27b}$$

Combination of these two results leads to

$$\tau_b = \frac{\tau_\lambda}{\tau_r \tau_c} \, . \tag{A 28}$$

Second,

$$M_9^2 = \frac{2}{(\gamma - 1)} \left[\left(\frac{P_9}{P_{s0}} \right)^{(\gamma-1)/\gamma} - 1 \right] = \frac{2}{(\gamma - 1)} \left[(\pi_r \pi_c \pi_t)^{(\gamma-1)/\gamma} - 1 \right] = \frac{2}{(\gamma - 1)} \left(\tau_r \tau_c \tau_t - 1 \right) . \tag{A 29}$$

Third,

$$\left(\frac{a_9}{a_0} \right)^2 = \frac{T_{s9}}{T_{s0}} = \frac{T_9}{T_{s0}} \left(\frac{P_{s0}}{P_9} \right)^{(\gamma-1)/\gamma} = \tau_b = \frac{\tau_\lambda}{\tau_r \tau_c} \, . \tag{A 30}$$

A.8.2 ***Bypass Flow*** The results corresponding to the core-flow Eqs. (A 29) and (A 30) for the bypass flow are

$$M_{19}^2 = \frac{2}{(\gamma - 1)} \left(\tau_r \tau_f - 1 \right) , \tag{A 31}$$

$$\left(\frac{a_{19}}{a_0} \right)^2 = \frac{T_{s19}}{T_{s0}} = \frac{T_{19}}{T_{s0}} \left(\frac{P_{s0}}{P_{19}} \right)^{(\gamma-1)/\gamma} = 1 \, . \tag{A 32}$$

The latter result, showing that the static temperature at the fan-stream exit and in the freestream are equal, is a non-obvious and slightly surprising result.

A.8.3 ***Rate-of-Mechanical-Work Balance*** The rate at which the fan and compressor needs mechanical work must equal the rate at which the turbine produces work. Consequently,

$$(1 + \alpha)(T_{13} - T_2) + T_3 - T_{21} = T_4 - T_5 \, , \tag{A 33}$$

which can be recast as

$$\tau_t = 1 - \frac{\tau_r}{\tau_\lambda} \left[\tau_c - 1 + \alpha (\tau_f - 1) \right] . \tag{A 34}$$

Thus, satisfying the power requirements determines the total-temperature ratio across the turbine in terms of the bypass ratio, fan- and compressor-design parameters and other set parameters.

A.8.4 *Ideal Thermal Efficiency* Since there is no net mechanical shaft work, the usual definition of thermal efficiency as being the ratio of the rates at which work is extracted and heat is added is not applicable for a turbofan, or a turbojet. Rather, the thermal efficiency, η_T, is defined as the net increase in the kinetic energy flux divided by the rate of heat addition, i.e.,

$$\eta_T = \frac{\Delta\dot{K}}{\dot{Q}}\,, \tag{A 35}$$

where $\Delta\dot{K}$ denotes the net increase in kinetic energy flux across the engine. The rate at which heat is added is simply

$$\dot{Q} = \dot{m} f h_{PR} = \frac{\dot{m} a_0^2}{\gamma - 1}(\tau_\lambda - \tau_\mathrm{r}\tau_\mathrm{c})\,, \tag{A 36}$$

where the last step follows from Eq. (A 27b) and the definition of the adiabatic speed of sound. The net increase in the kinetic energy flux is given by

$$\Delta\dot{K} = \frac{\dot{m}}{2}\left[V_9^2 + \alpha V_{19}^2 - (1+\alpha)V_0^2\right] = \frac{\dot{m} a_0^2}{2}\left[M_9^2\left(\frac{a_9}{a_0}\right)^2 + \alpha M_{19}^2\left(\frac{a_{19}}{a_0}\right)^2 - (1+\alpha)M_0^2\right]. \tag{A 37}$$

Combination of Eqs. (A 29)–(A 32), (A 36), and (A 37), after some algebraic manipulation, yields

$$\Delta\dot{K} = \dot{Q}\left(1 - \frac{1}{\tau_\mathrm{r}\tau_\mathrm{c}}\right). \tag{A 38}$$

It follows from Eqs. (A 35) and (A 38) that

$$\eta_T = 1 - \frac{1}{\tau_\mathrm{r}\tau_\mathrm{c}} = 1 - \left(\frac{1}{\pi_\mathrm{r}\pi_\mathrm{c}}\right)^{(\gamma-1)/\gamma}, \tag{A 39}$$

i.e., the thermal efficiency of a turbofan only depends on the product $\pi_\mathrm{r}\pi_\mathrm{c}$, which is usually referred to as the overall compression ratio, OCR. The higher the OCR the more thermally efficient the turbofan, or more precisely its core, becomes. Note that the OCR is not the same as the OPR, which is sometimes incorrectly implied during discussions of core thermal efficiency. The correct statement in this regard is: For a fixed flight Mach number, a larger OPR leads to higher core thermal efficiency.

Note that Eq. (A 39) also holds true for ideal turbojets. For a turbofan, part of the available kinetic-energy flux increase, created by the compression and combustion, is siphoned off to drive the fan, but is fully added back into the fan stream in the ideal case. For the turbojet all is added to the single nozzle flow.

A.8.5 *Ideal-Turbofan Equations* The turbofan-thrust formula, Eq. (A 11), becomes for the ideal cycle

$$F = \dot{m} a_0 \sqrt{\frac{2}{\gamma - 1}}\,\mathscr{F}\left(\tau_\lambda, \tau_\mathrm{r}, \tau_\mathrm{c}, \tau_\mathrm{f}, \alpha\right), \tag{A 40a}$$

where

$$\mathscr{F}\left(\tau_\lambda, \tau_\mathrm{r}, \tau_\mathrm{c}, \tau_\mathrm{f}, \alpha\right) = \sqrt{\tau_\lambda \eta_T - \tau_\mathrm{r}[\tau_\mathrm{c} - 1 + \alpha(\tau_\mathrm{f} - 1)]} + \alpha\sqrt{\tau_\mathrm{r}\tau_\mathrm{f} - 1} - (1+\alpha)\sqrt{\tau_\mathrm{r} - 1}\,. \tag{A 40b}$$

The first two terms in Eq. (A 40b) are associated with the thrust contributions from the core and fan streams, respectively, and the third term with the so-called inlet ram drag. Note that for fixed values of the other parameters/variables in Eq. (A 40b), there is an upper limit for the bypass ratio α. This limit, say α_ul, is obtained by the requirement that the argument inside the first radical (square root) in Eq. (A 40b) must not become negative, i.e.,

$$\alpha_\mathrm{ul} = \frac{1 + \eta_T\tau_\lambda/\tau_\mathrm{r} - \tau_\mathrm{c}}{\tau_\mathrm{f} - 1}\,. \tag{A 41}$$

There is another possible upper limit for α, which is obtained by requiring that the turbine total-temperature ratio is a positive number. Equation (A 34) shows that this limit would correspond to Eq. (A 41) with $\eta_T \equiv 1$, which can be rejected as the upper limit since $\eta_T \leq 1$.

The thrust-specific fuel consumption (TSFC) is defined as

$$S = \frac{f\dot{m}}{F}\,. \tag{A 42}$$

The fuel-air ratio is obtained from the last two members of Eq. (A 36), i.e.,

$$f = \frac{a_0^2}{(\gamma-1)h_{PR}}(\tau_\lambda - \tau_\mathrm{r}\tau_\mathrm{c})\,. \tag{A 43}$$

Substitution of Eqs. (A 40a) and (A 43) into Eq. (A 42) yields

$$S = \frac{a_0\,(\tau_\lambda - \tau_\mathrm{r}\tau_\mathrm{c})}{\sqrt{2(\gamma-1)}\,h_{PR}\mathscr{F}\,(\tau_\lambda, \tau_\mathrm{r}, \tau_\mathrm{c}, \tau_\mathrm{f}, \alpha)}\,. \tag{A 44}$$

The results in Eqs. (A 40), (A 43), and (A 44) all depend on the freestream speed of sound, i.e., on the ambient conditions through the temperature $T_{\mathrm{s}0}$.

A.8.6 ***Ideal Propulsive and Overall Efficiencies*** The propulsive efficiency, η_P, is defined as

$$\eta_P = \frac{FU_0}{\Delta\dot{K}}\,, \tag{A 45}$$

which after using Eq. (A 35) becomes

$$\eta_P = \frac{FU_0}{\eta_T\dot{Q}}\,. \tag{A 46}$$

Substituting Eqs. (A 36) and (A 40) into Eq. (A 46) then gives

$$\eta_p = \frac{2\sqrt{\tau_\mathrm{r}-1}}{\eta_T(\tau_\lambda - \tau_\mathrm{r}\tau_\mathrm{c})}\mathscr{F}\,(\tau_\lambda, \tau_\mathrm{r}, \tau_\mathrm{c}, \tau_\mathrm{f}, \alpha)\,. \tag{A 47}$$

The overall efficiency is given by

$$\eta_O = \eta_T\eta_P = \frac{2\sqrt{\tau_\mathrm{r}-1}}{\tau_\lambda - \tau_\mathrm{r}\tau_\mathrm{c}}\mathscr{F}\,(\tau_\lambda, \tau_\mathrm{r}, \tau_\mathrm{c}, \tau_\mathrm{f}, \alpha)\,. \tag{A 48}$$

It is instructive to note that the efficiencies, η_T, η_P, and η_O only depend on the flight Mach number (through τ_r), the design parameter τ_c and for the latter two also on the design parameter τ_f, the limit parameter τ_λ and the bypass ratio α. There is no explicit or implicit dependency on the ambient conditions.

A.8.7 ***Optimal Bypass Ratio*** By maximizing the function $\mathscr{F}\,(\tau_\lambda, \tau_\mathrm{r}, \tau_\mathrm{c}, \tau_\mathrm{f}, \alpha)$ with respect to α, the maximum thrust for a given core mass flow rate and the minimum TSFC are obtained (for any particular set of the other variables). Taking the partial derivative of Eq. (A 40) and equating the result to zero, shows that the extrema is located at

$$\alpha_\mathrm{opt} = \alpha_\mathrm{ul} - \frac{\left(\sqrt{\tau_\mathrm{r}\tau_\mathrm{f}-1}+\sqrt{\tau_\mathrm{r}-1}\right)^2}{4\tau_\mathrm{r}(\tau_\mathrm{f}-1)} = \frac{\eta_T\tau_\lambda - \tau_\mathrm{r}(\tau_\mathrm{c}-1) - \frac{1}{4}\left(\sqrt{\tau_\mathrm{r}\tau_\mathrm{f}-1}+\sqrt{\tau_\mathrm{r}-1}\right)^2}{\tau_\mathrm{r}(\tau_\mathrm{f}-1)}\,. \tag{A 49}$$

Note that $\alpha = \alpha_\mathrm{opt}$ also optimizes both the propulsive and overall efficiencies.

After some algebraic manipulation, it follows that

$$\mathscr{F}\left(\tau_\lambda, \tau_\mathrm{r}, \tau_\mathrm{c}, \tau_\mathrm{f}, \alpha_\mathrm{opt}\right) = (\alpha_\mathrm{opt} + \tfrac{1}{2})\left(\sqrt{\tau_\mathrm{r}\tau_\mathrm{f}-1} - \sqrt{\tau_\mathrm{r}-1}\right)\,, \tag{A 50}$$

where $\alpha_{\rm opt}$ is obtained from Eq. (A 49). In view of Eqs. (A 20b), (A 31), (A 32), and (A 40a), it follows that the thrust at the bypass-ratio optimum is

$$F_{\alpha=\alpha_{\rm opt}} = \dot{m}(\alpha_{\rm opt} + \tfrac{1}{2})(U_{19} - U_0)\,. \tag{A 51}$$

In addition, using Eqs. (A 29), (A 30), and (A 34) shows that

$$U_9 = \tfrac{1}{2}(U_{19} + U_0)\,, \tag{A 52}$$

which can immediately be rewritten as

$$\frac{U_9 - U_0}{U_{19} - U_0} = \frac{1}{2}\,. \tag{A 53}$$

Equation (A 53) also follows directly by combining the approximate form of Eq. (A 11) with Eq. (A 51. Equation (A 53) implies that the optimum bypass ratio leads to an inverted exit velocity profile, i.e., the fan exhaust has a larger velocity than the core nozzle. This situation is normally not implemented in practice!

A.8.8 ***Optimal Compression Ratio*** By taking the partial derivative of Eq. (A 40b) with respect to $\tau_{\rm c}$, it follows that an optimum is obtained for

$$(\tau_{\rm r}\tau_{\rm c})_{\rm opt} = \sqrt{\tau_\lambda}\,, \tag{A 54}$$

which is easily shown to correspond to a maximum value of $\mathscr{F}$ by a second partial differentiation. Hence, the corresponding optimal overall compression ratio is known for a given value of the design-limitation parameter τ_λ. It is not very likely, except under very special circumstances, that a design will be carried out under the constraint Eq. (A 54). However, it leads to the rule of thumb that $\tau_\lambda \sim (\tau_{\rm r}\tau_{\rm c})^2$, i.e., a scaling law giving a rough estimate of what temperature T_4 is optimally needed for a desired overall compression ratio.

A.8.9 ***Corrected or Referred Quantities*** As already pointed out, the results in Eqs. (A 40), (A 43), and (A 44) for the thrust, fuel-air ratio, and thrust-specific fuel consumption, respectively, depend on the ambient conditions through the temperature $T_{\rm s0}$. It is customary (as well as expedient) to relate these results to those for a specific reference condition, namely the sea-level standard (SLS), or sometimes referred to as (standard) sea-level static conditions,

$$P_{\rm SLS} = 101.325\,kPa\,, \tag{A 55a}$$

$$T_{\rm SLS} = 288.15\,K\,. \tag{A 55b}$$

The actual ambient pressure and temperature can then be normalized as

$$\delta_{\rm s0} = \frac{P_{\rm s0}}{P_{\rm SLS}}\,, \tag{A 56a}$$

$$\theta_{\rm s0} = \frac{T_{\rm s0}}{T_{\rm SLS}}\,. \tag{A 56b}$$

The actual core mass flow rate, thrust, and thrust-specific fuel consumption for given ambient conditions can now be related to those for SLS conditions by introducing

$$\dot{m}^* = \frac{\dot{m}\sqrt{\theta_{\rm s0}}}{\delta_{\rm s0}}\,, \tag{A 57a}$$

$$F^* = \frac{F}{\delta_{\rm s0}} = \dot{m}^*\sqrt{2c_pT_{\rm SLS}}\,\mathscr{F}\,, \tag{A 57b}$$

$$S^* = \frac{S}{\sqrt{\theta_{\rm s0}}} = \sqrt{\frac{c_pT_{\rm SLS}}{2}}\,\frac{\tau_\lambda - \tau_{\rm r}\tau_{\rm c}}{h_{PR}\mathscr{F}}\,, \tag{A 57c}$$

where the star superscript, '*', denotes quantities corrected to SLS conditions. This particular notation is judged superior here since the (often used) subscripts 'c' or 'r' are already used in this report for other purposes.

Normally a component analysis, say for a compressor stage, produces results in terms of corrected variables based on component-inlet conditions. In general, the total pressure ratio across a rotating component is of the form [14, 15]

$$\pi = \pi(\dot{m}^*_{\mathrm{a}}, N^*_{\mathrm{a}}), \tag{A 58}$$

where

$$\dot{m}^*_{\mathrm{a}} \equiv \frac{\dot{m}\sqrt{\theta_{\mathrm{a}}}}{\delta_{\mathrm{a}}} = \frac{P_{\mathrm{SLS}} A_{\mathrm{a}}}{\sqrt{R T_{\mathrm{SLS}}}} \mathscr{M}(\gamma_{\mathrm{a}}, M_{\mathrm{a}}) \tag{A 59a}$$

and

$$N^*_{\mathrm{a}} \equiv \frac{N}{\sqrt{\theta_{\mathrm{a}}}} = \frac{\sqrt{R T_{\mathrm{SLS}}}}{r_{\mathrm{a}}} \sqrt{\frac{\gamma_{\mathrm{a}}}{1 + \frac{\gamma_{\mathrm{a}}-1}{2} M^2_{\mathrm{a}}}}\, M_{\mathrm{Ta}} \tag{A 59b}$$

are corrected mass flow rate and shaft speed, based on the stagnation properties at the component-inlet station ‘a’;

$$\mathscr{M}(\gamma, M) = \frac{\sqrt{\gamma} M}{\left(1 + \frac{\gamma-1}{2} M^2\right)^{\frac{\gamma+1}{2(\gamma-1)}}} \tag{A 59c}$$

is a nondimensional mass flow parameter;

$$M_{\mathrm{Ta}} = \frac{r_{\mathrm{a}} N}{\sqrt{\gamma_{\mathrm{a}} R T_{\mathrm{sa}}}} \tag{A 59d}$$

is the tip Mach number of the first rotor (radius r_{a}) in the component; and

$$\delta_{\mathrm{a}} = \frac{P_{\mathrm{a}}}{P_{\mathrm{SLS}}}, \tag{A 59e}$$

$$\theta_{\mathrm{a}} = \frac{T_{\mathrm{a}}}{T_{\mathrm{SLS}}}. \tag{A 59f}$$

are the component-inlet normalized total pressure and total temperature. Equation (A 58) is a generic representation of the component performance map. The mass flow parameter $\mathscr{M}$ strictly speaking depends on both the ratio of the specific heats and the Mach number, but the former can often be taken as a constant, as is assumed here. Hence, the corrected mass flow rate per unit area $\dot{m}^*_{\mathrm{a}}/A_a$ is only a function of the axial Mach number to lowest order of approximation. Note that the function $\mathscr{M}$ increases monotonically with the Mach number M until it reaches a maximum for $M = 1$ and decreases thereafter. In view of Eqs. (A 59a–d), the total pressure ratio across the component can alternatively be characterized in terms of its inlet axial and rotor-tip Mach numbers.

A.9 *Component Matching*

The ideal cycle analysis, so far, has considered the design parameters as independent, see A.7. However, the matching of the turbofan components through mass flow and shaft-speed requirements establishes relationships between these parameters. In general, this is accomplished by using so-called component maps (that relate pressure ratios to mass flow rates and shaft speeds) in combination with inter-component power requirements. This is an iterative procedure that determines what is known as the pumping characteristics of the gas-turbine engine. However, a common simplification in an ideal analysis is to assume that the flow is choked at several internal-flow-path locations. Having a flow path choked at more than one location places serious restrictions on the parameter dependencies, but greatly simplifies the analysis. Fortunately, this is a reasonable assumption in practice [15, § 8.1.2, p. 440] for wide range of (higher) engine-throttle settings.

A.9.1 *High-Pressure Turbine Inlet Guide Vanes* Turbofan aeroengines are commonly designed such that the flow is choked, or nearly so, at the minimum flow area of the HPT inlet guide vanes (IGV) over a large range of engine operational points. Denoting this effective HPT-IGV area as A_4, it follows that the ideal core mass flow rate is

$$\dot{m} = \rho_{\mathrm{s}4} \sqrt{\gamma R T_{\mathrm{s}4}}\, A_4 = \frac{P_4 \Gamma_4 A_4}{\sqrt{R T_4}} = \frac{\pi_r \pi_c P_{\mathrm{s}0}}{\sqrt{R \tau_\lambda T_{\mathrm{s}0}}} \Gamma_4 A_4, \tag{A 60}$$

where Γ_4 denotes the value at station 4 of the function

$$\Gamma(\gamma) = \sqrt{\gamma}\left(\frac{2}{\gamma+1}\right)^{\frac{\gamma+1}{2(\gamma-1)}} . \tag{A 61}$$

Note that Eq. (A 61) is simply the mass flow parameter Eq. (A 59c) evaluated at a choked-flow location. Combining Eqs. (A 57a) and (A 60) shows that the referred HPT-IGV-choked core mass flow rate is

$$\dot{m}^* = \frac{P_{\mathrm{SLS}} A_4}{\sqrt{R T_{\mathrm{SLS}}}} \frac{\pi_r \pi_c \Gamma_4}{\sqrt{\tau_\lambda}} . \tag{A 62}$$

In reality, Γ_4 depends weakly on T_{s4}, but it is assumed to be constant in the idealized analysis. Equation (A 62) shows that the choked mass flow rate at the IGV, referred to the standard sea-level-static conditions, only depends on the flight Mach number through the ram pressure ratio, π_r. If, on the other hand, the HPT-IGV conditions are used as the basis for the corrected core mass flow rate, one obtains

$$\dot{m}_4^* = \frac{P_{\mathrm{SLS}} \Gamma_4 A_4}{\sqrt{R T_{\mathrm{SLS}}}} \tag{A 63}$$

which shows that the corrected mass flow rate per unit area, $\dot{m}_4^*/A_4$, is constant.

A.9.2 ***Core-Nozzle Throat*** The turbofan core nozzle is often designed such that it is sonic at the throat, i.e., at station 8 (Fig. A 1). It then follows that

$$\dot{m} = \rho_{8s}\sqrt{\gamma R T_{s8}}\, A_8 = \frac{P_8 \Gamma_8 A_8}{\sqrt{R T_8}} = \frac{\pi_r \pi_c \pi_t P_{s0}}{\sqrt{R \tau_\lambda \tau_t T_{s0}}} \Gamma_8 A_8 . \tag{A 64}$$

Combining Eqs. (A 60) and (A 64), followed by some simple manipulations, shows that for an ideal turbine

$$\tau_t = \left(\frac{\Gamma_4 A_4}{\Gamma_8 A_8}\right)^{\frac{2(\gamma-1)}{\gamma+1}} = \left(\frac{A_4}{A_8}\right)^{\frac{2(\gamma-1)}{\gamma+1}} , \tag{A 65a}$$

$$\pi_t = \left(\frac{\Gamma_4 A_4}{\Gamma_8 A_8}\right)^{\frac{2\gamma}{\gamma+1}} = \left(\frac{A_4}{A_8}\right)^{\frac{2\gamma}{\gamma+1}} , \tag{A 65b}$$

i.e., as long as both the IGV and the core-nozzle throat both remain choked, the turbine operates at a fixed point that is simply defined by the flow-area ratio of the HPT IGV and the core-nozzle throat.

A.9.3 ***Low-Pressure Turbine Inlet Guide Vanes*** If the flow is also (approximately) choked at the minimum flow area of the LPT IGV for the engine conditions considered above, it follows that the ideal corrected core mass flow rate based on the LPT-IGV conditions is

$$\dot{m}_{45}^* = \frac{P_{\mathrm{SLS}} A_{45} \Gamma_{45}}{\sqrt{R T_{\mathrm{SLS}}}} , \tag{A 66}$$

where A_{45} is the effective LPT-IGV area. By introducing separate total temperature and total pressure ratios for the HPT and LPT (denoted by the subscripts 'Ht' and 'Lt'), it follows that

$$\tau_{Ht} = \left(\frac{A_4}{A_{45}}\right)^{\frac{2(\gamma-1)}{\gamma+1}} , \tag{A 67a}$$

$$\pi_{Ht} = \left(\frac{A_4}{A_{45}}\right)^{\frac{2\gamma}{\gamma+1}} , \tag{A 67b}$$

$$\tau_{Lt} = \left(\frac{A_{45}}{A_8}\right)^{\frac{2(\gamma-1)}{\gamma+1}}, \tag{A 67c}$$

$$\pi_{Lt} = \left(\frac{A_{45}}{A_8}\right)^{\frac{2\gamma}{\gamma+1}}, \tag{A 67d}$$

with $\tau_t = \tau_{Ht}\tau_{Lt}$ and $\pi_t = \pi_{Ht}\pi_{Lt}$. Since the total pressure ratios for both turbines are fixed (set by effective flow-area ratios) and their inlet corrected mass flow rates are both constant, each turbine operates at a single point in their respective maps. This means that the (local, or component-based) corrected shaft speed for each turbine is constant.

A.9.4 ***Corrected Fan Speed*** The concept of engine power is not quite relevant for a turbofan or turbojet,[i] consequently the operation of of such aeroengines are usually characterized in terms of its fan speed, or more precisely the ratio of its corrected fan speed to the corresponding ADP value. The actual fan speed, N_{F}, is directly proportional to (or, if the fan is not geared, equal to) the actual low-pressure-spool shaft speed, N_{L}. Thus, $N^*_{\mathrm{F}45}$, the corrected fan speed based on the LPT inlet conditions, is a constant. It follows that the corrected fan speed, based on fan-face conditions,

$$N^*_{\mathrm{F}2} = \frac{N_{\mathrm{F}}}{\sqrt{\theta_2}} = N^*_{\mathrm{F}45}\sqrt{\frac{\theta_{45}}{\theta_{\mathrm{s}0}}} = N^*_{\mathrm{F}45}\sqrt{\frac{T_{45}}{T_0}} = N^*_{\mathrm{F}45}\sqrt{\frac{\tau_\lambda\,\tau_{Ht}}{\tau_r}}\left(\frac{A_4}{A_{45}}\right)^{\frac{\gamma-1}{\gamma+1}}. \tag{A 68}$$

Since both $N^*_{\mathrm{F}45}$ and τ_{Ht} are constants, Eq. (A 68) shows that the corrected fan speed only depends on the square root of the temperature ratio T_4/T_0 and, because of this, it is a good indicator of the engine-operational point. As a pilot increases the throttle setting, more fuel is injected and T_4 increases.

Equation (A 68) implies

$$\frac{\tau_\lambda}{\tau_r} = \left(\tau_\lambda/\tau_r\right)_{\mathrm{ADP}}\left(N^*_{\mathrm{F}2}/N^*_{\mathrm{F}2_{\mathrm{ADP}}}\right)^2, \tag{A 69}$$

where the subscript 'ADP' indicates the value of a quantity at the aerodynamical-design point. As long as the core flow path remains choked at the HPT-IGV, LPT-IGV, and core-nozzle throat locations, the temperature ratio T_4/T_0 depends only on the square of the corrected fan speed normalized by its value at the ADP. The value of the design parameter $\tau_{\lambda_{\mathrm{ADP}}}$ can be set by

$$\tau_{\lambda_{\mathrm{ADP}}} = \min\left[T_{4_{\mathrm{lim}}}/T_{\mathrm{s}0_{\mathrm{ADP}}}, (\tau_r\tau_c)^2_{\mathrm{ADP}}\right], \tag{A 70}$$

or by some other criteria deemed better by the turbofan designer. The first and second arguments on the right-hand side of Eq. (A 70) represent a material temperature limitation and the optimum value for a given OCR at the ADP, respectively. As will be seen later in the report, Eq. (A 69), with Eq. (A 70) or equivalent, characterizes the engine operational performance in terms of $N^*_{\mathrm{F}2}/N^*_{\mathrm{F}2_{\mathrm{ADP}}}$.

A.9.5 ***Fan-Nozzle Throat*** In general, the fan-stream nozzle is also designed to be sonic at its throat (station 18 in Fig. A 1) at the ADP conditions. In an ideal situation, as considered here, the stagnation properties at this location are equal to those at station 13 as well as those at station 21. Again assuming that the choked assumption remains approximately valid for the operating conditions of interest leads to

$$\alpha\dot{m} = \rho_{\mathrm{s}18}\sqrt{\gamma R T_{\mathrm{s}18}}A_{18} = \frac{P_{18}\Gamma_{18}A_{18}}{\sqrt{RT_{18}}} = \frac{\pi_r\pi_f P_{\mathrm{s}0}}{\sqrt{R\tau_r\tau_f T_{\mathrm{s}0}}}\Gamma_{18}A_{18}. \tag{A 71}$$

Combining Eqs. (A 60) and (A 71) shows that the bypass ratio is given by

$$\alpha = \frac{1}{\pi_{Hc}}\sqrt{\frac{\tau_\lambda}{\tau_r\tau_f}}\,\frac{\Gamma_{18}A_{18}}{\Gamma_4 A_4} = \frac{1}{\pi_{Hc}}\sqrt{\frac{\tau_\lambda}{\tau_r\tau_f}}\,\frac{A_{18}}{A_4}, \tag{A 72}$$

where $\pi_{Hc} = \pi_c/\pi_f = P_3/P_{21}$ is the total pressure ratio for the HPC.

---

[i] For a turboshaft engine, the shaft power is a well defined measure of performance, however.

A.9.6 *High-Pressure-Compressor Operating Line* The corrected mass flow rate at the inlet of the high-pressure compressor, i.e., at station 21, is given by

$$\dot{m}^*_{21} = \frac{\dot{m}\sqrt{\theta_{21}}}{\delta_{21}} = \frac{P_{\mathrm{SLS}}\Gamma_4 A_4}{\sqrt{RT_{\mathrm{SLS}}}} \frac{\pi_{Hc}}{\sqrt{T_4/T_{21}}} \tag{A 73}$$

Thus, for a given $T_4/T_{21} = \tau_\lambda/(\tau_r\tau_f)$, Eq. (A 73) represents a straight-line relationship between $\dot{m}^*_{21}$ and π_{Hc} that passes through the origin. However, Eq. (A 73) does not hold near the origin since the assumption that the core-flow path remains nearly choked at all the required locations is not valid in that region. In addition, T_4/T_{21} does not remain constant as the HPC operation point changes. At least one additional relationship is needed to establish the HPT performance. By combining the mechanical-power balance between the HPC and the HPT, i.e., $T_3 - T_{21} = T_4 - T_{45}$, with Eq. (A 67a) one obtains

$$\frac{\tau_\lambda}{\tau_r\tau_f} = \frac{T_4}{T_{21}} = \frac{\pi_{Hc}^{\frac{\gamma-1}{\gamma}} - 1}{1 - (A_4/A_{45})^{\frac{2(\gamma-1)}{\gamma+1}}} \,. \tag{A 74}$$

Combination of Eqs. (A 73) and (A 74) then yields the HPC operating line[j]

$$\dot{m}^*_{21} = \frac{P_{\mathrm{SLS}}\Gamma_4 A_4}{\sqrt{RT_{\mathrm{SLS}}}}\, \pi_{Hc} \sqrt{\frac{1 - (A_4/A_{45})^{\frac{2(\gamma-1)}{\gamma+1}}}{\pi_{Hc}^{\frac{\gamma-1}{\gamma}} - 1}} \,. \tag{A 75}$$

In practice, the key challenge for a compressor designer is then to construct a device where this line is contained within a region of high efficiencies and also has a sufficient distance from the compressor stall line. A further discussion of this particular topic is beyond the scope of this report, however.

Combination of Eqs. (A 72) and (A 74) gives

$$\alpha = \frac{1}{\pi_{Hc}} \sqrt{\frac{\pi_{Hc}^{\frac{\gamma-1}{\gamma}} - 1}{1 - (A_4/A_{45})^{\frac{2(\gamma-1)}{\gamma+1}}}}\, \frac{A_{18}}{A_4} \,, \tag{A 76}$$

which shows that the BPR depends only on the high-pressure-compressor total-pressure ratio for an ideal-cycle turbofan under choked-flow conditions.

A.9.7 *Fan Operating Line* The corrected fan mass flow rate, based on the fan-face conditions (station 2), is given by

$$\dot{m}^*_{12} = (1+\alpha)\dot{m}^*_2 = \frac{\pi_f}{\sqrt{\tau_f}}(1+\alpha)\dot{m}^*_{21} = \pi_f^{\frac{\gamma+1}{2\gamma}}(1+\alpha)\dot{m}^*_{21} = \tau_f^{\frac{\gamma+1}{2(\gamma-1)}}(1+\alpha)\dot{m}^*_{21} \,, \tag{A 77}$$

where $\dot{m}^*_{21}$ and α are given by Eqs. (A 75) and (A 76), respectively. Note that $\dot{m}^*_{21}$ and α only depend on π_{Hc}. Since the total-pressure ratios for both the high-pressure compressor and the fan will change with the turbofan operation, a relationship between π_{Hc} and π_f (or τ_f) needs to be determined.

The mechanical-power balance between the fan and the LPT, i.e., $(1+\alpha)(T_{21} - T_2) = T_{45} - T_5$, yields

$$1 + \alpha = \frac{\tau_{Ht}(1-\tau_{Lt})\tau_\lambda}{\tau_r(\tau_f - 1)} = \frac{(A_4/A_{45})^{\frac{2(\gamma-1)}{\gamma+1}}\,[1 - (A_{45}/A_8)^{\frac{2(\gamma-1)}{\gamma+1}}]\tau_\lambda}{\tau_r(\tau_f - 1)} \,, \tag{A 78}$$

where Eqs. (A 67a,c) were used in the last step. Combining Eqs. (A 76) and (A 78) produces

$$\frac{1 - (A_4/A_{45})^{\frac{2(\gamma-1)}{\gamma+1}}}{\pi_{Hc}^{\frac{\gamma-1}{\gamma}} - 1} + \frac{1}{\pi_{Hc}} \sqrt{\frac{1 - (A_4/A_{45})^{\frac{2(\gamma-1)}{\gamma+1}}}{\pi_{Hc}^{\frac{\gamma-1}{\gamma}} - 1}}\, \frac{A_{18}}{A_4} = (A_4/A_{45})^{\frac{2(\gamma-1)}{\gamma+1}}\,[1 - (A_{45}/A_8)^{\frac{2(\gamma-1)}{\gamma+1}}]\,\frac{\tau_f}{\tau_f - 1} \,, \tag{A 79}$$

which is the needed relationship between π_{Hc} and τ_f. Thus, Eqs. (A 75)–(A 77) and (A 79) define the fan operating line.

---

[j] This result is also the corresponding compressor operating line for a turbojet

A.10 *Engine Geometry*

The ideal-cycle analysis in Section A.8, does not involve any specific geometry information for the turbofan engine. Many therefore consider that stage of the analysis as representing a 'rubber' engine, i.e., where the areas at the different engine stations simply adjust themselves in response to the provided parameters. However, the combination of the component matching, described in Section A.9, with the desired ADP properties then determines (at least) some of the engine geometry.

Equation (A 65), which is a consequence of the flow being choked at two locations in the core flow path, gives

$$\frac{A_4}{A_8} = (\tau_{t,\mathrm{ADP}})^{\frac{\gamma+1}{2(\gamma-1)}} = (\pi_{t,\mathrm{ADP}})^{\frac{\gamma+1}{2\gamma}} \,. \tag{A 80a}$$

Equation (A 74), describing the mechanical-power balance between the HPC and HPT, yields

$$\frac{A_4}{A_{45}} = \left[1 - \frac{\tau_r\tau_f}{\tau_\lambda}(\tau_{Hc}-1)\right]_{\mathrm{ADP}}^{\frac{\gamma+1}{2(\gamma-1)}} \,. \tag{A 80b}$$

It then follows that

$$\frac{A_{45}}{A_8} = (\frac{A_4}{A_8})/(\frac{A_4}{A_{45}}) = \left[\frac{\tau_t}{1-\frac{\tau_r\tau_f}{\tau_\lambda}(\tau_{Hc}-1}\right]_{\mathrm{ADP}}^{\frac{\gamma+1}{2(\gamma-1)}} \,. \tag{A 80c}$$

Finally, Eq. (A 72), which is valid when both the HPT IGV and fan-nozzle throat are choked, shows that

$$\frac{A_4}{A_{18}} = \left[\frac{1}{\alpha\pi_{Hc}}\sqrt{\frac{\tau_\lambda}{\tau_r\tau_f}}\right]_{\mathrm{ADP}} \,. \tag{A 80d}$$

Note that for the rotating components, the total-pressure and the corresponding total-temperature ratios are related through the isentropic relationship, Eq. (A 18). Consequently, the ratio giving the 'cleanest' formulas is used above.

From the definition of the corrected mass flow rate at a station, i.e., Eq. (A 59a), and Eq. (A 63) it follows that

$$A_4 = \frac{\sqrt{RT_{\mathrm{SLS}}}}{P_{\mathrm{SLS}}\Gamma_4}\left[\dot{m}_3^*\sqrt{\frac{\tau_\lambda}{\tau_r\tau_c}}\right]_{\mathrm{ADP}} \,. \tag{A 81}$$

Since Eq. (A 81) determines the area A_4, the areas A_{45}, A_8, and A_{18} are consequently known through the area-ratio results in Eq. (A 80).

The fan-face area, A_2, is also of particular interest since it is an essential ingredient in establishing the engine nacelle diameter, which is important for engine-installation considerations. Combination of Eqs. (A 59a) and (A 77), using Eqs. (A 73), and (A 74), produces

$$A_2\mathscr{M}_{2_{\mathrm{ADP}}} = A_4\left[\Gamma_4(1+\alpha)\pi_c\sqrt{\frac{\tau_r}{\tau_\lambda}}\right]_{\mathrm{ADP}} \,, \tag{A 82}$$

where $\mathscr{M}_2 = \mathscr{M}(\gamma_2, M_2)$ denotes the value of the function defined by Eq. (A 59c) at station 2. Equation (A 82), rather than defining the area A_2, in actuality determines the Mach number M_2 that the inlet has to 'deliver' at the fan face for a given value of A_2. A discussion of inlet-design principles is well beyond the scope of this report, except for stating that a subsonic inlet is supposed to raise the static pressure and static temperature of the stream by reducing the flow velocity so as to reduce the Mach number to the required $M_2 < M_0$.

A.11 *Off-Design Performance*

As is commonly conjectured, the turbofan off-design performance is obtained by assuming that the turbofan flow stays approximately choked at all the locations previously discussed. It follows that

$$\pi_t = \pi_{t_{\mathrm{ADP}}} \,, \quad \tau_t = \tau_{t_{\mathrm{ADP}}} = \pi_{t_{\mathrm{ADP}}}^{\frac{\gamma-1}{\gamma}} \,, \tag{A 83}$$

with analogous expressions for π_{Ht}, τ_{Ht}, π_{Lt}, and τ_{Lt}, since the turbines operate at a fixed point as long as the HPT-IGV, LPT-IGV, and core-nozzle throat remain choked. The fan-LPT, HPC-HPT and overall mechanical-power balances imply that

$$(1+\alpha)(\tau_f - 1) = \frac{\tau_\lambda}{\tau_r}\tau_{Ht_{\text{ADP}}}(1-\tau_{Lt_{\text{ADP}}}), \tag{A 84a}$$

$$\tau_f(\tau_{Hc} - 1) = \frac{\tau_\lambda}{\tau_r}(1-\tau_{Ht_{\text{ADP}}}), \tag{A 84b}$$

$$(1+\alpha)(\tau_f - 1) + \tau_f(\tau_{Hc} - 1) = \frac{\tau_\lambda}{\tau_r}(1-\tau_{t_{\text{ADP}}}). \tag{A 84c}$$

Note that Eqs. (A 84) are not linearly independent since adding the first two sub-equations produces the third, which, of course, is directly understandable from the physics involved. Rearranging Eq. (A 84b) to obtain an expression for τ_f in terms of the other variables and then substituting this result into Eq. (A 84a) yields

$$\frac{\tau_\lambda}{\tau_r} = \frac{1+\alpha}{(1+\alpha)(1-\tau_{Ht_{\text{ADP}}})/(\tau_{Hc}-1) - \tau_{Ht_{\text{ADP}}}(1-\tau_{Lt_{\text{ADP}}})}. \tag{A 85}$$

Equation (A 85), in combination with Eq. (A 76), allows the determination of τ_λ/τ_r as a function of π_{Hc}, i.e., π_{Hc} is known in terms of τ_λ/τ_r through an implicit relationship. Hence, the bypass ratio α, is also known in terms of τ_λ/τ_r through Eq. (A 76). Equation (A 84b) then is used to obtain τ_f as a function of τ_λ/τ_r. Thus, the OPR, $\pi_c = \pi_f \pi_{Hc}$, dependency on τ_λ/τ_r is determined.

Since, $\dot{m}_4^*$ is constant, and equal to the value in Eq. (A 63), it follows that the corrected core mass flow rate at the HPC exit is given by

$$\dot{m}_3^* = \dot{m}_{4_{\text{ADP}}}^* \sqrt{\frac{\tau_r \tau_c}{\tau_\lambda}} = \frac{P_{\text{SLS}}\Gamma_4 A_4}{\sqrt{RT_{\text{SLS}}}} \sqrt{\frac{\tau_r \tau_c}{\tau_\lambda}}. \tag{A 86a}$$

Similarly, the corrected core mass flow rate based on fan-face conditions is

$$\dot{m}_2^* = \dot{m}_{4_{\text{ADP}}}^* \pi_c \sqrt{\frac{\tau_r}{\tau_\lambda}} = \frac{P_{\text{SLS}}\Gamma_4 A_4}{\sqrt{RT_{\text{SLS}}}} \pi_c \sqrt{\frac{\tau_r}{\tau_\lambda}}. \tag{A 86b}$$

Furthermore, it turns out that the corrected total-temperature increase across the combustor, based on fan-face conditions,

$$(\Delta T)_2^* \equiv \frac{T_4 - T_3}{\theta_2} = T_{\text{SLS}}\left(\frac{\tau_\lambda}{\tau_r} - \tau_c\right), \tag{A 87}$$

is a function only of τ_λ/τ_r as well.

In view of Eq. (A 69), it follows that all the variable quantities discussed in this section, such as π_f, π_{Hc}, π_c, $\dot{m}_2^*$, $\dot{m}_3^*$, and $(\Delta T)_2^*$ only depend on the corrected fan speed. That is, the parameter $N_{\text{F2}}^*/N_{\text{F2}_{\text{ADP}}}^*$ characterizes the off-design performance of the turbofan.

A.12 *Some Other Useful Relationships*

Two parameters that are usually displayed on the cockpit instrument panel in order to inform the pilots, and to aid them in the aircraft operation, are the exit gas temperature, EGT, and the engine pressure ratio, EPR. In terms of the variables used herein, they are

$$\text{EGT} = T_5 \tag{A 88a}$$

$$\text{EPR} = P_5/P_2. \tag{A 88b}$$

Under the ideal assumptions, the turbines, HPT and LPT, each operate at fixed point, i.e., the turbine total-temperature ratio is constant over a wide variety of throttle settings. The EGT is then directly proportional to T_4, the combustor-exit total temperature. Hence, the EGT is an indicator of the end result of the combustion process.

Nozzles are usually characterized in terms of their pressure ratio, NPR, which is the ratio of their inlet total pressure and the static pressure at their exit. For a given nozzle, the NPR determines its ideal exit velocity. For the core and fan nozzles, it follows that

$$\text{NPR}_C = P_5/P_{\text{s}0} = \pi_r \,\text{EPR}, \tag{A 89a}$$

$$\text{NPR}_F = P_{13}/P_{\text{s}0} = \pi_r \,\text{FPR}. \tag{A 89b}$$

B ANOPP-GECOR Combustor-Noise Model

B.1 *General Discussion*

The combustor-noise prediction in NASA ANOPP [5, 6] is provided by the GECOR subroutine. This module essentially contains two basic semi-empirical models with options. The first model is fully 1/3-octave based and in its original implementation [7, 8] is customarily referred to as the SAE method. There are, however, some subtle differences in how the SAE method is implemented in ANOPP GECOR compared to the original formulation [9, Section 8 and Appendix D], see Refs. [10, 11] for a discussion. The GECOR module also contains a small-engine revision [18] (referred to as SmE herein) as well as an option for an alternate turbine-transmission-loss formula [19–23]. The second class of models, that will not be further discussed, has an intermediate-narrowband formulation [24] in order to account for tail-pipe resonances.

A characteristic feature of most models for combustor noise is that the farfield directivity and spectral distribution are decoupled. This is the case for both the SAE and SmE methods in ANOPP GECOR. For a moving source in a media at rest, the (dimensional) combustor-noise mean-square pressure in each frequency band (b) detected by an observer at rest is given by

$$< p^2 >^{(b)} = \frac{\rho_m c_m \Pi D(\phi_e) S(f_e^{(b)})}{4\pi R_e^2 (1 - M_0 \cos\phi_e)^4} F_{AA}(R_e, f_m^{(b)}), \tag{B 1a}$$

where ρ_m and c_m are the ambient density and speed of sound at the observer (measurement) location, R_e is the distance the sound wave has traveled to reach the observer, and the $(1 - M_0 \cos\phi_e)^{-4}$ factor is referred to as Mach amplification; $f_e^{(b)}$ is a center-band frequency in the moving-source frame of reference (also referred to as the emission frequency) and

$$f_m^{(b)} = \frac{f_e^{(b)}}{1 - M_0 \cos\phi_e} \tag{B 1b}$$

is the corresponding Doppler-shifted frequency sensed by the stationary observer as well as experienced by the air molecules during the sound-wave propagation. Π is the total radiated acoustic power by the source; $D(\phi_e)$ is a directivity function that depends only on the emission polar angle ϕ_e and satisfies the normalization condition

$$\int_0^\pi D(\phi) \sin\phi \, \mathrm{d}\phi = 2; \tag{B 1c}$$

$S(f_e^{(b)})$ is a spectrum function satisfying

$$\sum_b S(f_e^{(b)}) = 1. \tag{B 1d}$$

The multiplicative-factor $F_{AA}(R_e, f_m^{(b)})$ in Eq. (B 1a) represents the atmospheric attenuation as a sound wave travels from the source to the observer. The notation is a bit simplified since in addition to the distance traveled by and the Doppler-shifted frequency of the sound wave, the attenuation also depends on the ambient static temperature and humidity experienced during propagation. However, in the absence of atmospheric attenuation and in a frame of reference moving with the source, the total radiated acoustic power through a sphere surrounding the source with the radius R_m is given by

$$\int_A \frac{\sum_b < p^2 >^{(b)}}{\rho_m c_m} \mathrm{d}A = \Pi, \tag{B 2}$$

where $\mathrm{d}A = R_m^2 \sin\phi_e \mathrm{d}\phi_e \mathrm{d}\theta_e$, with θ_e denoting the azimuthal angle. That is, the total radiated acoustic power Π is preserved as the acoustic waves propagate away from the source if atmospheric attenuation is negligible.

Note that the formulation in Eq. (B 1) is equally valid for a narrowband or fractional-octave-band description of the phenomena. The spectrum function in the latter case simply is obtained by assigning the narrowband values of the former to the correct fractional-octave band. The ANOPP-GECOR SAE and SmE models use 1/3-octave frequency bands. It is important to realize that the Doppler effect, Eq. (B 1b), shifts both the frequency and size of each band at the observer location compared to the corresponding values at the source. This spectral rearrangement depends on both the flight Mach number and the emission polar angle.

Figure B 1 illustrates the relationship between emission-time and reception-time coordinates for a source moving with a constant velocity U_0 and rate-of-climb angle β. The subscripts 'e' and 'r' indicate variables associated with the

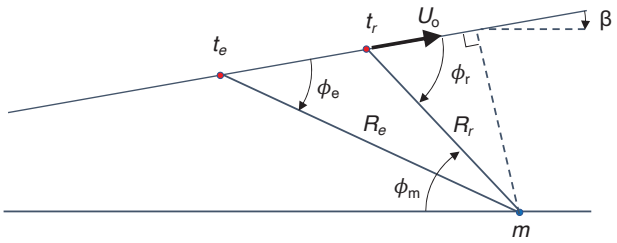

Figure B 1. Emission-Time and Reception-Time Coordinates for a source moving at speed U_0

emission point and the source location when the sound wave is received at the measurement (observer) location 'm', respectively. Geometric manipulations show that

$$R_e(1 - M_0 \cos\phi_e) = R_r\sqrt{1 - M_0^2 \sin^2\phi_r}\,, \tag{B 3a}$$

$$\cos\phi_e = \frac{\cos\phi_r + M_0\sqrt{1 - M_0^2\sin^2\phi_r}}{M_0\cos\phi_r + \sqrt{1 - M_0^2\sin^2\phi_r}}\,, \tag{B 3b}$$

where

$$\phi_r = \phi_m + \beta\,. \tag{B 3c}$$

Equations (B 3a,b) define the emission-time coordinates in terms of the reception-time coordinates—the latter can be assumed to be known from the flyover event—and correspond to the results in Crighton et al. [25, Eqs. 14.22 and 14.23].

The ANOPP-GECOR formula for the total acoustic power emitted by the source is

$$\Pi = 10^{K/10} c_0^2 \dot{m} \left(\frac{T_4 - T_3}{T_3}\right)^2 \left(\frac{P_3}{P_{s0}}\right)^2 F_{TA}\,, \tag{B 4a}$$

where the constant $K = -60.53\ldots$ in the SAE method and $K = -64.53\ldots$ in the SmE method. Using the notation defined in Appendix A, $\dot{m}$ is the mass flow rate into the combustor, T_3 and T_4 are the total temperature at the combustor inlet and exit, P_3 is the total combustor-inlet pressure, and c_0 and P_{s0} are the ambient speed of sound and (static) pressure at the source location. *Note that the only difference between the SAE and SmE methods is the value of the constant K leading to a 4 dB difference in the acoustic power level!*

The factor F_{TA} in Eq. (B 4a) accounts for turbine attenuation, or loss, and, in the original formulation [26], is given by

$$F_{TA} = \left(\frac{\Delta T_{ADP}}{T_{s0}}\right)^{-4}\,, \tag{B 4b}$$

where ΔT_{ADP} is the design-point total temperature drop across the turbine[k] and T_{s0} is the ambient (static) temperature at the source location. Note that the acoustic transmission loss is independent of the engine operating condition with this formulation. The GECOR module has been updated to also have an option to use an alternative turbine-transmission-loss formula, namely the simplified [21] Pratt & Whitney [19, 20] acoustic-turbine-loss formula,

$$F_{TA} = \frac{0.8\zeta}{(1+\zeta)^2}\,, \tag{B 4c}$$

where ζ is the ratio of the characteristic impedances across the turbine, i.e. $\zeta = \rho_{s5}c_5/\rho_{s4}c_4$, see Fig. A 1. With this formulation, the turbine acoustic transmission loss depends on the engine operation conditions since the impedance ratio does. Hultgren [22][l] found that predictions using this formula compared well with data for flight idle, approach,

[k] If this value is not available, the corresponding takeoff value can be used.

[l] Due to a typographical error, Eq. 13 in Hultgren [22] corresponding to Eq. (B 4c) here is inverted, but the computations therein are correct.

cutback, and takeoff power settings from a full-scale static-engine test [27]. Equations (B 4b) and (B 4c) here are referred to as the GE and PW turbine-transmission-loss formulas, respectively. Note that both these loss formulas are frequency independent.

B.2 *Rescaled Acoustic Power*

Using the results of Appendix Section A.8 recasts Eq. (B 4a) for the total emitted acoustic power into

$$\Pi = 10^{K/10}\frac{\gamma R}{T_{\mathrm{s0}}}\left(\frac{fh_{PR}}{\bar{c}_p}\right)^2 \dot{m}\,(\pi_r\pi_c)^{\frac{2}{\gamma}}\,F_{TA} = \delta_{\mathrm{s0}}\sqrt{\theta_{\mathrm{s0}}}\,10^{K/10}\frac{\gamma R}{T_{\mathrm{SLS}}}\left(\frac{fh_{PR}}{\bar{c}_p\theta_{\mathrm{s0}}}\right)^2 \dot{m}_3^*\,(\pi_r\pi_c)^{\frac{\gamma+5}{2\gamma}}\,F_{TA}\,, \tag{B 5}$$

where $fh_{PR}/\bar{c}_p = \Delta T$ (the total temperature increase across the combustor). The notation $\bar{c}_p$ is used to clarify that this constant-pressure specific heat represents an average, or representative, value for the combustor. In the ideal-cycle analysis of Appendix A, the simplified assumption is made that c_p is constant throughout the whole turbofan flow path, however. Equation (B 5) shows that the emitted acoustic power is proportional to the corrected core mass flow rate at the compressor exit and to the overall-compression ratio raised to the power $(\gamma+5)/(2\gamma) = 8/3.5$.

REFERENCES

[1] Mongeau, L., Huff, D. and Tester, B. J. "Aircraft Noise Technology Review and Medium and Long Term Noise Reduction Goals." *ICA 2013 Montreal*. 2013. DOI 10.1121/1.4800944.

[2] Burley, C. L., Rawls, Jr, J. W., Berton, J. J. and Marcolini, M. A. "Aircraft System Noise Prediction." Dahl, M. D. (ed.). *Assessment of NASA's Aircraft Noise Prediction Capability*. NASA/TP-2012-215653 (2012): Chap. 2, pp. 11–33.

[3] Berton, J. J., Envia, E. and Burley, C. L. "An Analytical Assessment of NASA's N+1 Subsonic Fixed Wing Project Noise Goal." AIAA Paper 2009-3144. 16th AIAA/CEAS Aerocoustics Conference, Miami, Florida. 2009. DOI 10.2514/6.2009-3144.

[4] Lylte, J. K. "The Numerical Propulsion Sysytem Simulation: An Overview." Technical Report No. NASA/TM–2000-209915. NASA. 2000. URL `https://ntrs.nasa.gov/citations/20000063377`.

[5] Zorumski, W. E. "Aircraft Noise Prediction Program Theoretical Manual, Part 1." Technical Report No. NASA-TM-83199-PT-1. NASA. 1982.

[6] Zorumski, W. E. "Aircraft Noise Prediction Program Theoretical Manual, Part 2." Technical Report No. NASA-TM-83199-PT-2. NASA. 1982.

[7] Emmerling, J. J., Kazin, S. B. and Matta, R. K. "Core Engine Noise Control Program, Volume III, Supplement 1—Prediction Methods." Technical Report No. FAA-RD-74-125 III-I (AD A030376). FAA. 1976.

[8] Ho, P. Y. and Doyle, V. L. "Combustion Noise Prediction Update." AIAA Paper 1979-0588. 5th AIAA Aerocoustics Conference, Seattle, Washington. 1979. DOI 10.2514/6.1979-588.

[9] Society of Automotive Engineers International. "Gas Turbine Jet Exhaust Prediction." Technical Standard (Aerospace Recommended Practice) SAE ARP876 Rev. E. 2006 (Reaffirmed 2012). DOI 10.4271/ARP876E.

[10] Hultgren, L. S. "Semi-Empirical Modeling and Prediction of Direct Combustor Noise." Technical Report No. NASA/TM–2018-220041. NASA. 2018.

[11] Tam, C. K. W, Bake, F., Hultgren, L. S. and Poinsot, T. "Combustion Noise: Modeling and Prediction." *CEAS Aeronautical J.* Vol. 10 No. 1 (2019): pp. 101–122. DOI 10.1007/s13272-019-00377-2.

[12] McCormick, D., Snyder, J., Kim, W. and Mendoza, J. M. "Acoustics of Future Low-Emissions Combustor Technology, Volume 1: Final Report." Contractor Report NASA/CR-20205011099/VOL1. NASA. 2020. URL `https://ntrs.nasa.gov/citations/20205011099`.

[13] Hultgren, L. S. "Core-Noise: Implications of Emerging N+3 Designs and Acoustic Technology Needs." 2011. Acoustics Technical Working Group, Cleveland, Ohio, NASA E-17796. URL `https://ntrs.nasa.gov/archive/nasa/casi.ntrs.nasa.gov/20110011393.pdf`.

[14] Kerrebrock, J. L. *Aircraft Engines and Gas Turbines*, 2nd ed. MIT Press (1992). URL `https://mitpress.mit.edu/contributors/jack-l-kerrebrock`.

[15] Mattingly, J. D. *Elements of Propulsion Gas Turbines and Rockets*. AIAA (2006). DOI 10.2514/4.103711.

[16] Society of Automotive Engineers International. "Gas Turbine Engine Performance Station Identification and Nomenclature." Technical Standard (Aerospace Recommended Practice) SAE ARP755A. 1974 (Reaffirmed 2011). DOI 10.4271/ARP755A.

[17] "U. S. Standard Atmosphere 1976." Technical Report No. NASA-TM-X-34335 (NOAA-S/T-76-1562). NASA/NOAA/USAF. 1976. URL https://ntrs.nasa.gov/citations/19770009539.

[18] Hough, J. W and Weir, D. S. "Small Engine Technology (SET)—Task 13 ANOPP Noise Prediction for Small Engines: Jet, Core, and Turbine Module Revisions." Technical Report No. No. 21-9655. AlliedSignal Engines, Phoenix, Arizona. 1997.

[19] Mathews, D. C., Rekos, Jr, N. F. and Nagel, R. T. "Combustion Noise Investigation." Technical Report No. FAA-RD-77-3. FAA. 1977.

[20] Mathews, D. C. and Rekos, Jr, N. F. "Prediction and Measurement of Direct Combustion Noise in Turbopropulsion Systems." *J. Aircraft* Vol. 14 No. 9 (1977): pp. 850–859. DOI 10.2514/3.58865.

[21] Mahan, R. J. and Karchmer, A. "Combustion and Core Noise." Hubbard, H. H. (ed.). *Aeroacoustics of Flight Vehicles: Theory and Practice*. Vol. 1. NASA Reference Publication 1258, WRDC Technical Report 90-3052 (1991): Chap. 9, pp. 483–517.

[22] Hultgren, L. S. "Full-Scale Turbofan-Engine Turbine-Transfer Function Determination Using Three Internal Sensors." AIAA Paper 2011-2912 (NASA/TM-2012-217252). 17th AIAA/CEAS Aeroacoustic Conference, Portland, Oregon. 2011. DOI 10.2514/6.2011-2912.

[23] Hultgren, L. S. "A Comparison of Combustor-Noise Models." AIAA Paper 2012-2087 (NASA/TM-2012-217671). 18th AIAA/CEAS Aerocoustics Conference, Colorado Springs, Colorado. 2012. DOI 10.2514/6.2012-2087.

[24] Schuster, B. and Lieber, L. "Narrowband Model for Gas Turbine Engine Combustion Noise Prediction." AIAA Paper 2006-2677. 12th AIAA/CEAS Aerocoustics Conference, Cambridge, Massachusetts. 2006. DOI 10.2514/6.2006-2677.

[25] Crighton, D. G., Dowling, A. P., Ffowcs Williams, J. E., Heckl, M. and Leppington, F. G. *Modern Methods in Analytical Acoustics: Lecture Notes*. Springer-Verlag, Berlin (1992).

[26] Motsinger, R. "Prediction of Engine Combustor Noise and Correlation with T64 Engine Low Frequency Noise." Technical Report No. R72AEG313. General Electric Co. 1972.

[27] Weir, D. S. "Engine Validation of Noise and Emission Reduction Technology Phase I." Technical Report No. NASA/CR-2008-215225. NASA. 2008. Honeywell Report No. 21-13843, Honeywell Aerospace, Phoenix, Arizona.